Nicotine exploits a COPI-mediated process for chaperone-mediated up-regulation of its receptors

Brandon J. Henderson,[1] Rahul Srinivasan,[1] Weston A. Nichols,[1] Crystal N. Dilworth,[1] Diana F. Gutierrez,[1] Elisha D.W. Mackey,[1] Sheri McKinney,[1] Ryan M. Drenan,[2] Christopher I. Richards,[3] and Henry A. Lester[1]

[1]Division of Biology and Biological Engineering, California Institute of Technology, Pasadena, CA 91125
[2]Department of Medicinal Chemistry and Molecular Pharmacology, Purdue University, West Lafayette, IN 47907
[3]Department of Chemistry, University of Kentucky, Lexington, KY 40506

Chronic exposure to nicotine up-regulates high sensitivity nicotinic acetylcholine receptors (nAChRs) in the brain. This up-regulation partially underlies addiction and may also contribute to protection against Parkinson's disease. nAChRs containing the α6 subunit (α6* nAChRs) are expressed in neurons in several brain regions, but comparatively little is known about the effect of chronic nicotine on these nAChRs. We report here that nicotine up-regulates α6* nAChRs in several mouse brain regions (substantia nigra pars compacta, ventral tegmental area, medial habenula, and superior colliculus) and in neuroblastoma 2a cells. We present evidence that a coat protein complex I (COPI)-mediated process mediates this up-regulation of α6* or α4* nAChRs but does not participate in basal trafficking. We show that α6β2β3 nAChR up-regulation is prevented by mutating a putative COPI-binding motif in the β3 subunit or by inhibiting COPI. Similarly, a COPI-dependent process is required for up-regulation of α4β2 nAChRs by chronic nicotine but not for basal trafficking. Mutation of the putative COPI-binding motif or inhibition of COPI also results in reduced normalized Förster resonance energy transfer between α6β2β3 nAChRs and εCOP subunits. The discovery that nicotine exploits a COPI-dependent process to chaperone high sensitivity nAChRs is novel and suggests that this may be a common mechanism in the up-regulation of nAChRs in response to chronic nicotine.

The Journal of General Physiology

INTRODUCTION

One of the earliest discoveries of chronic nicotine exposure was the observation of an increased number of nicotinic acetylcholine receptors (nAChRs; termed up-regulation) (Marks et al., 1983; Schwartz and Kellar, 1983; Breese et al., 1997; Mamede et al., 2007; Nashmi et al., 2007). Classically, up-regulation of nAChRs has been defined as an increase in nAChR protein, as identified by increased agonist binding (Marks et al., 1983; Benwell et al., 1988; Flores et al., 1992; Peng et al., 1994), but we now define up-regulation as a change in receptor number, stoichiometry, and trafficking (Lester et al., 2009; Miwa et al., 2011). Often, an increase in total binding as opposed to cell surface binding has been reported. Therefore, up-regulation of nAChRs involves an increase in nAChR abundance throughout the cell (ER, Golgi, etc.) and not exclusively on the plasma membrane (PM). There have been several hypotheses regarding the mechanism of up-regulation, but a consensus is emerging that nicotine acts inside the cell to enhance a critical step(s) in the maturation process of nAChRs (Sallette et al., 2005). This intracellular enhancement process has been characterized as pharmacological chaperoning (Kuryatov et al., 2005; Lester et al., 2009), and it occurs at the nanomolar concentrations thought to persist in the brain for hours after a person smokes. Research from many laboratories indicates that up-regulation of α4β2 nAChRs occurs through a similar process in human brains, animal brains, cultured neurons, and clonal transfected cell lines (Nashmi et al., 2007; Mukhin et al., 2008; Miwa et al., 2011; Srinivasan et al., 2011; Lester et al., 2012).

Up-regulation of nAChRs in response to chronic nicotine plays a major role in nicotine dependence and, perhaps, in the inverse correlation between a person's history of tobacco use and his or her susceptibility to Parkinson's disease (Ritz et al., 2007; Koob, 2009). Individual deletions of the α4, α6, or β2 nAChR subunits are sufficient to block the self-administration of nicotine in mice (Pons et al., 2008), whereas the selective reexpression of these deleted subunits in the ventral tegmental area (VTA) is sufficient to reinstate self-administration of nicotine (Pons et al., 2008; Brunzell et al., 2010).

Correspondence to Henry A. Lester: Lester@Caltech.edu

Abbreviations used in this paper: COPI, coat protein complex I; ERES, ER exit sites; nAChR, nicotinic acetylcholine receptor; Neuro-2a, neuroblastoma 2a; NFRET, normalized Förster resonance energy transfer; PM, plasma membrane; PMID, PM integrated density; ROI, regions of interest; SEP, supercliptic-pHluorin; SNc, substantia nigra pars compacta; TIRFM, total internal reflection fluorescence microscopy; VTA, ventral tegmental area.

The Rockefeller University Press $30.00
J. Gen. Physiol. Vol. 143 No. 1 51–66
www.jgp.org/cgi/doi/10.1085/jgp.201311102

Furthermore, nicotine self-administration can be blocked by the selective antagonism of α6* (*, IUPHAR nomenclature, "other subunits may be present") (Jackson et al., 2009) or α4* (Yoshimura et al., 2007) nAChRs. From this, it is clear that the nAChRs mediating nicotine addiction include those that contain α4, α6, and β2 subunits (Picciotto et al., 1998; Tapper et al., 2004; Pons et al., 2008).

Despite the clarity of α4β2 nAChR up-regulation, there have been conflicting reports of up-regulation, down-regulation, or no change in response to chronic nicotine for α6* nAChRs (Tumkosit et al., 2006; Perez et al., 2008; Walsh et al., 2008). Here, we used mice expressing α6–enhanced green fluorescence protein (eGFP) nAChR subunits to test for in vivo up-regulation of α6* nAChRs using concentrations of nicotine comparable to those produced by smoking in humans. We determined that this up-regulation occurs in all four brain areas that robustly express α6* nAChRs: the VTA, the substantia nigra pars compacta (SNc), the medial habenula, and the superior colliculus.

We then used α6 subunits tagged with superclipticpHluorin (SEP), a pH-sensitive eGFP analogue, expressed in neuroblastoma cells to analyze the mechanism of α6* nAChR up-regulation. SEP has been used to study vesicle dynamics and synaptic delivery (Miesenböck et al., 1998; Mani and Ryan, 2009) as well as the trafficking of AMPA and GABA receptors (Jacob et al., 2005; Jaskolski et al., 2009; Lin et al., 2009; Araki et al., 2010), and we have used α4-SEP* to study nAChR trafficking after chronic exposure to nicotine (Richards et al., 2011). Here, we show that nicotine-induced up-regulation fails to occur with inhibition of coat protein complex I (COPI)-mediated retrograde traffic from the Golgi to the ER (either through the mutation of a putative COPI-binding motif [β3-KKK] or through the use of the COPI inhibitor CI-976). COPI is a protein complex that coats vesicles for retrograde transport of proteins from the cis end of the Golgi to the ER (Brandizzi and Barlowe, 2013). COPI is a heptameric protein complex, and di-lysine–trafficking motifs, including KKxx and KxKxx, facilitate protein binding to COPI (Jackson et al., 2012; Spang, 2013). Inhibition of COPI-mediated trafficking resulted in a decrease of nAChR density in the ER and a complementary increase of nAChR density in the Golgi. Inhibition of COPI had no effect on basal insertion of nAChRs in the PM but prevented their up-regulation during chronic nicotine treatment. Therefore, we propose that the cycling of nAChRs between the Golgi and ER (via COPI) is necessary for the up-regulation of α4β2 and α6β2β3 nAChRs. Our data suggest that this may be a common mechanism of nAChR up-regulation by nicotine, and that the manipulation of Golgi–ER cycling may lead to novel therapeutic strategies for nicotine cessation or neuroprotection against Parkinson's disease.

MATERIALS AND METHODS

Reagents

The β-COP antibody (rabbit polyclonal) was obtained from Abcam (AB2899). CI-976 and (−)-nicotine hydrogen tartrate were obtained from Sigma-Aldrich.

Mice and chronic nicotine administration

The construction of α6-GFP mice has been described previously (Mackey et al., 2012). All experiments were conducted in accordance with the guidelines for care and use of animals provided by the National Institutes of Health, and protocols were approved by the Institutional Animal Care and Use Committee at the California Institute of Technology.

Chronic nicotine administration

Mice were kept on a standard 12-h light/dark cycle at 22°C and given food and water ad libitum. Chronic nicotine or saline was administered to mice using miniosmotic pumps (model 2002; Alzet). On the day of pump implantation, saline or (−)-nicotine hydrogen tartrate (Sigma-Aldrich) was prepared freshly and loaded into the pump to deliver nicotine at 2 mg/kg/h or 0.4 mg/kg/h. This concentration provides maximal nAChR up-regulation and a peripheral blood concentration that is near the peak concentration found in the blood of human smokers (Marks et al., 2004). Surgical procedures for the pump implantation have been reported previously (Nashmi et al., 2007).

Cell culture

Mouse neuroblastoma 2a (Neuro-2a) cells were cultured using standard techniques (Xiao et al., 2011). Cells were plated by adding 90,000 cells to poly-D-lysine–coated 35-mm glass-bottom imaging dishes (MatTek Corporation) and cultured in a humidified incubator (37°C, 95% air, 5% CO_2). Cells were transfected with 500 ng of each nAChR subunit plasmid and 250 ng GalT-mCherry or Sec24D-mCherry for assays. Plasmids were mixed with 250 µl Opti-MEM. Lipofectamine-2000 was separately added to 250 µl Opti-MEM. After 5 min at 24°C, DNA and Lipofectamine solutions were mixed together and incubated for 25 min at 24°C. The solutions were then added to preplated Neuro-2a cells and incubated for 24 h. After 24 h, the Opti-MEM was removed and replaced with growth medium. 50 or 500 nM of filter-sterilized nicotine was added after replacing the Opti-MEM with standard culture medium (α6β2β3 nAChRs). For α4β2 nAChRs, 100 nM nicotine was used for 48 h (nicotine was added at the time of transfection and then replenished when the media was changed). 20 µM CI-976 was added with nicotine 24 h before imaging. Cells were imaged 48 h after transfection.

Patch-clamp recordings

For patch-clamp electrophysiology, 50,000 Neuro-2a cells were plated onto sterilized 12-mm glass coverslips (Deckgläser), placed in 35-mm culture dishes, and cultured in a humidified incubator (37°C, 95% air, 5% CO_2). Recorded cells were visualized with an inverted fluorescence microscope (IX71; Olympus) in either bright field or fluorescence (eGFP) mode using a high pressure Hg lamp (HB-10103AF; Nikon). Electrophysiological signals were recorded with an amplifier (Axopatch-1D; Axon Instruments), analogue-to-digital converter (Digidata 1440A; Axon Instruments), and software (pClamp 10.0; Axon Instruments). Patch pipettes were filled with solution containing (mM): 135 K gluconate, 5 KCl, 5 EGTA, 0.5 $CaCl_2$, 10 HEPES, 2 Mg-ATP, and 0.1 GTP (pH was adjusted to 7.2 with Tris-base, and osmolarity was adjusted to 280–300 mOsm with sucrose). The resistance of patch pipettes was 2–4 MΩ for whole-cell recordings. Junction potential was nulled just before

forming a gigaseal. All recordings were done at 24°C. Data were sampled at 10 kHz and filtered at 2 kHz for whole-cell recordings. Acetylcholine was dissolved in extracellular solution containing (mM) 140 NaCl, 5 KCl, 2 $CaCl_2$, 1 $MgCl_2$, 10 HEPES, and 10 glucose (320 mOsm, pH set to 7.3 with Tris-base), and were puffed (0.3 s, 20 psi) onto voltage-clamped Neuro-2a cells (holding potential [V_H] of −50 mV). To avoid receptor desensitization by repetitive ACh application, we applied ACh at ∼3-min intervals and continually perfused the recording chamber with extracellular solution. For concentration response studies, we used a rapid superfusion system with 500-ms puffs of agonist (Octaflow II; ALA Scientific Instruments).

Immunostaining and antibodies

For immunostaining, cultured Neuro-2a cells were fixed with 4% paraformaldehyde (15 min), permeabilized in 0.01% Triton X-100 (5 min), and blocked with 10% goat serum (30 min). After two PBS washes, the appropriate primary antibody (1:500) in 1% goat serum was applied for 1 h at 24°C. Cells were washed three times with PBS and incubated with 1% goat serum containing secondary antibody (1:2,000) for 1 h at 24°C. Cells were washed three times with PBS and imaged immediately. Immunostaining used β-COP rabbit polyclonal antibody as the primary (antibody 2899; Abcam) and Alexa Fluor 555–labeled secondary (goat anti–rabbit; Invitrogen) antibodies.

Midbrain α6-GFP neurons existed in a high enough density to be imaged without staining (direct/inherent fluorescence). Immunohistochemical techniques were required for observing α6-GFP fluorescence in other regions of the mouse brain. 20-µm brain sections on slides were rinsed twice for 10 min with PBS and then permeabilized with 0.5% Triton X-100 in PBS for 1 h. Brain sections were then blocked with 4% goat serum (Jackson ImmunoResearch Laboratories, Inc.) in PBS for 45 min. The primary antibody was diluted in 4% goat serum in PBS and incubated overnight at 24°C. Brain sections were then washed three times for 15 min with PBS, and the secondary antibody was diluted in 4% goat serum in PBS and incubated for 1 h at 24°C. Finally, brain sections were washed three times for 15 min with PBS and mounted with Vectashield.

Total internal reflection fluorescence microscopy (TIRFM)

Cultured Neuro-2a cells were imaged live at 37°C in a stage-mounted culture dish incubator (Warner Instruments) using methods similar to TIRFM assays in cultured cortical neurons (Richards et al., 2011). TIRFM enables the visualization of fluorescently labeled intracellular molecules within ∼250 nm of the cell-coverslip interface. TIRFM images were obtained using an inverted fluorescence microscope (IX81; Olympus) equipped with a 100× 1.45 NA oil objective (PlanApo; Olympus) and a stepper motor (Thorlabs) to control the position of the fiber optic and TIRFM evanescent field illumination. Just before imaging, growth medium was exchanged for extracellular solution (150 mM NaCl, 4 mM KCl, 10 mM HEPES, 2 mM MgCl2, 2 mM CaCl2, and 10 mM glucose), adjusted to the appropriate pH (5.4 or 7.4). SEP was excited at 488 nm with an air-cooled argon laser (IMA101040ALS; Melles Griot). Images were captured with a back-illuminated EMCCD camera (iXon DU-897; Andor). We acidified the imaging dish by perfusing the bath, normally at pH 7.4, with an otherwise identical solution adjusted to pH 5.4. The PM integrated density (PMID) was determined by taking an initial TIRFM image of each cell at pH 7.4, followed by acidification of the solution and a subsequent low pH image (pH 5.4). Low pH images were used to demarcate ER-localized nAChRs, which were subtracted from the total footprint to determine the PMID of nAChRs. The figures show a single imaging session that is representative of at least three sessions performed on separate days with similar or identical results.

Insertion events were quantified using methods similar to those published previously (Richards et al., 2011). TIRFM measurements to detect membrane insertion events were performed with consecutive 200-ms frames. Insertion events were defined as punctate regions of fluorescence appearing at the membrane. Insertion event data are represented in terms of insertion per 10 μm^2 of area per minute of observation.

Spectral confocal imaging

Imaging experiments were performed in live Neuro-2a cells at 37°C in a stage-mounted culture dish incubator (Warner Instruments). For immunostaining, fixed Neuro-2a cells were imaged. A C1si laser-scanning confocal microscope (Eclipse; Nikon) equipped with a 60× 1.2 NA VC Plan Apo water objective and 32 photomultiplier tubes was used for confocal imaging. Before an imaging session, cell culture medium was replaced with phenol red–free CO_2-independent Leibovitz (L-15) medium (Invitrogen). eGFP and mCherry were excited at 488 and 561 nm, respectively. For each cell, we focused on a plane containing the most ER exit sites (ERES), Golgi bodies, or COPI vesicles, and sequential images of eGFP and mCherry fluorescence were obtained. eGFP and mCherry fluorescence emission spectra were captured and images were unmixed using standard spectra acquired from cells expressing eGFP, mCherry, or Alexa Fluor 555 alone. For quantification, ERES, Golgi, or COPI regions of interest (ROI) were manually demarcated using intensity-based thresholding, and the raw integrated densities were measured for each cell using ImageJ. The total Sec24D fluorescence in ERES and the total GalT fluorescence per cell were quantified. Error bars for measurements indicate the SEM, and p-values are based on a two-tailed *t* test. The figures show a single imaging session that is representative of at least three sessions performed on separate days with similar or identical results.

For direct fluorescence imaging of in vivo α6-GFP* nAChRs, images were acquired with the 60× 1.2 NA VC Plan Apo water objective at wavelengths between 496 and 561 nm using a 488-nm line of an argon laser. Images were collected at 12-bit intensity over 512 × 512 pixels, a resolution of 2.5 nm, a 61.3-µm pinhole, and a pixel dwell time of 8.4 µs. Autofluorescence was separated from GFP fluorescence using techniques that have been published previously (Nashmi et al., 2007). Image analysis of cell counts and mean intensities were done with ImageJ.

Normalized Förster resonance energy transfer (NFRET)

The general methods for Förster resonance energy transfer from sensitized acceptor emission have been described previously (Srinivasan et al., 2011, 2012a). For these studies, Neuro-2a cells were transfected with α6-mCherry, β2wt, εCOP-GFP, and β3wt or $\beta3_{AAA}$ nAChR subunits. Cells transfected with either α6-mCherry or εCOP-GFP alone were included in all imaging sessions to control for pixel saturation and spectral bleedthrough. Live cells were imaged with a C1si laser-scanning confocal microscope (Eclipse; Nikon). During acquisition of images, cells were focused on a plane where the εCOP-GFP fluorescence most resembled the pattern for the endogenous COPI staining (see Fig. 4 E). GFP and mCherry images were acquired with 488- and 561-nm laser lines, and images were linearly unmixed by using reference spectra. Reference spectra were acquired from Neuro-2a cells transfected with α6-mCherry or εCOP-GFP during the same imaging session. After linear unmixing, NFRET was calculated using the PixFRET ImageJ plug-in as described previously (Moss et al., 2009; Srinivasan et al., 2011, 2012a).

Plasmid constructs

Mouse α6 with a C-terminal fusion of an SEP tag was constructed by PCR amplification using the forward primer 5′-CATGGTTGGCTGGTATGATCAGTAAAGGAGAAGAACTT-3′ and the reverse primer 5′-ATGGATGAACTATACAAATAGGGAATAGCGGCACCT-3′,

which overlap with sequences within the C-terminal end of the α6-coding sequence. This PCR product was then cloned directly into the vector containing the α6 gene using Pfu-Turbo polymerase. The mouse $\beta2_{\beta3}$ nAChR subunit was constructed by PCR amplification using the forward primer 5′-ATGGCCCGGTGCTCCAACTC-3′ and the reverse primer 5′-CCTGCCCTCAGACTGTGGTG-3′. The mouse $\beta3_{\beta2}$ nAChR subunit was constructed by PCR amplification using the forward primer 5′-ATGACAGGCTTCCTACGGGT-3′ and the reverse primer 5′-ACGGTCCTGGTGTTCTACCT-3′. Mouse $\beta3_{AAA}$ (the KKK mutated to AAA) and the $\beta2_{\beta3[AAA]}$ were constructed by PCR amplification using the forward primer 5′-AAATTTCCAGGGGCTGCAGCCCAGACTCCTACC-3′ and the reverse primer 5′-CCCCCTCACGGTTCCCTTACTCTCCGT-3′.

Online supplemental material

Fig. S1 illustrates that the presence of β3 subunits increased the PMID of α6β4 nAChRs but is not required for the up-regulation of α6β4* nAChRs. Fig. S2 presents a schematic of the various chimeras and mutant nAChR subunits that were used in this paper. Fig. S3 shows the electrophysiological characterization of $\alpha6\beta2\beta3_{WT}$ and $\alpha6\beta2\beta3_{AAA}$ nAChRs after treatment with nicotine. Here, we show that functional up-regulation accompanies the increase in PMID for $\alpha6\beta2\beta3_{WT}$ nAChRs when treated with nicotine, but there is no functional up-regulation with $\alpha6\beta2\beta3_{AAA}$ nAChRs. Fig. S4 illustrates that treatment with CI-976 produces an increase of nAChRs in the Golgi but does not increase export from the ER. Fig. S5 shows that CI-976 treatment does not affect basal PMID of nAChRs. The online supplemental material is available at http://www.jgp.org/cgi/content/full/jgp.201311102/DC1.

RESULTS

In vivo up-regulation of α6* nAChRs with chronic nicotine

We used a mouse line containing GFP-labeled α6* nAChRs to study the up-regulation of α6* nAChRs (Mackey et al., 2012). α6-GFP nAChR subunits assemble appropriately with other nonlabeled nAChR subunits, traffic properly, and function in electrophysiological assays in a manner comparable to that of WT nAChRs (Mackey et al., 2012).

Direct fluorescence of α6-GFP* nAChRs was apparent in the VTA and SNc of saline- or nicotine-treated mice (Fig. 1 A). The fluorescence intensity of α6-GFP* nAChRs in the VTA and SNc of mice administered nicotine at 2 mg/kg/h for 10 d was increased twofold compared with that of saline-treated mice ($P < 0.005$; Fig. 1, B_1 and C_1). In addition, we used cumulative percentage plots to compare saline and nicotine treatments (Fig. 1, B_2 and C_2). Cumulative percentage plots are similar to a cumulative frequency analysis and allow us to compare the full range of α6-GFP fluorescence intensities between saline and nicotine treatments. In all four brain regions, we can see that the percentage of low, mid, and high α6-GFP fluorescence intensities are shifted to the right

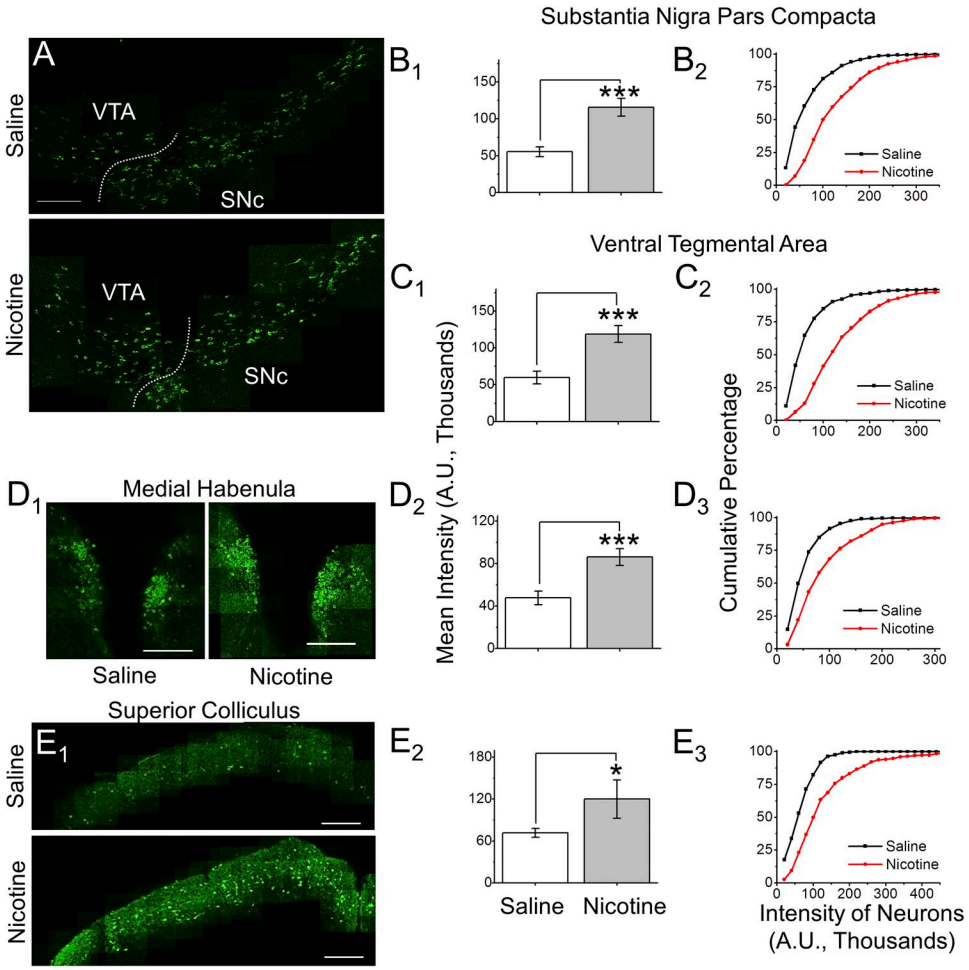

Figure 1. Chronic nicotine up-regulates α6-GFP* nAChRs in four brain regions. (A) Direct fluorescence imaging of SNc and VTA in mice expressing α6-GFP subunits after treatment with saline or nicotine (2 mg/kg/h, 10 d). (D_1 and E_1) Immunohistochemical imaging of medial habenula and superior colliculus in mice expressing α6-GFP subunits after treatment with saline or nicotine. For all images, montages were compiled from individual 60× images. (A and E_1) Bars, 100 µm. (D_1) Bars, 20 µm. (B_1 and C_1) Quantification of α6-GFP intensities in SNc and VTA of saline- and nicotine-treated mice ($n = 6$ mice). (D_2 and E_2) Quantification of α6-GFP intensities in medial habenula and superior colliculus of saline- and nictotine-treated mice ($n = 6$ mice). (D_3 and E_3) Quantification of α6-GFP immunofluorescence of medial habenula and superior colliculus neurons in saline- and nicotine-treated mice ($n = 4$–5 mice). (B_2, C_2, D_3, and E_3) Cumulative percentage plots show changes in α6-GFP fluorescence in all brain regions with chronic nicotine. ***, $P < 0.005$; *, $P < 0.05$.

(higher intensity) after chronic nicotine treatment (Fig. 1, B_2 and C_2). Nicotine at 0.4 mg/kg/h also increased α6-GFP fluorescence intensity in VTA (60.8 ± 10.9% increase) and SNc (70.0 ± 1.4% increase) neurons ($P < 0.05$ compared with saline; Fig. 2). Similar to 2 mg/kg/h nicotine treatments, the 0.4-mg/kg/h nicotine treatment shifted the full range of α6-GFP fluorescence intensities to the right in cumulative percentage plots (Fig. 2, D_1 and D_2).

2 mg/kg/h nicotine also increased the fluorescence intensity of medial habenula and superior colliculus α6-GFP* nAChRs (81% [$P < 0.005$] and 68% [$P < 0.05$], respectively; Fig. 1, D and E). In cumulative percentage plots, we can also see that the full range of α6-GFP fluorescence intensities is shifted to the left after chronic nicotine treatment (Fig. 1, D_1 and D_2).

α6-SEP* nAChRs assemble functional receptors, and β3 subunits increase α6* nAChR function

To perform a systematic study on α6* nAChR up-regulation, we used an expression system, Neuro-2a cells, which has been optimized to avoid many artifacts of "overexpressing" PM proteins. The appearance of functional PM proteins in this system is linear and unsaturated as a function of parameters such as level of transfected cDNAs, trafficking machinery, oligomerization, and anchoring (Moss et al., 2009).

SEP undergoes 488-nm excitation at neutral pH (~7.4) but not under acidic conditions (Richards et al., 2011). α6-SEP* nAChRs in the Golgi and secretory vesicles (~6.7 and <6.5 pH, respectively) are not fluorescent (Asokan and Cho, 2002; Jaskolski et al., 2009). When exposed to a neutral buffer (pH ~7.4) both ER- and PM-resident nAChRs are fluorescent. Upon perfusing an acidic buffer (pH 5.4), PM-resident nAChR fluorescence is quenched, whereas the ER component remains fluorescent. Thus, SEP allows the differentiation of receptors within the ER from those in the PM. As in a previous study using SEP tagged to α4 nAChRs (Richards et al., 2011), we fused SEP to the C terminus of α6 subunits so that it was positioned on the luminal side of organelles in the secretory pathway.

nAChRs with eGFP subunits have little or no functional difference (i.e., peak current amplitude, decay time) from WT subunits (Drenan et al., 2008; Richards et al., 2011; Srinivasan et al., 2011, 2012b; Xiao et al., 2011) and, indeed, we found no detectable functional difference between α6-SEPβ2β3 nAChRs and α6-eGFPβ2β3 nAChRs (Fig. 3). Inclusion of the β3 subunit increased ACh-induced peak currents by threefold compared with those obtained with α6-eGFPβ2 nAChRs (Fig. 3 B; $P < 0.05$). Inclusion of the β3 subunit also reduced the concentration of ACh at which we observed maximal peak amplitude from 300 µM (α6-eGFPβ2) to 3 µM (α6-eGFPβ2β3) (Fig. 3). Concentration–response studies of ACh and (−)-nicotine on α6-eGFPβ2β3 nAChRs yielded EC_{50} values of 0.31 ± 0.10 µM and 0.12 ± 0.08 µM, respectively (Fig. 3, C and D), which agree with those obtained with linked concatamers containing $(α6β2)_2β3$ nAChRs (Kuryatov and Lindstrom, 2011).

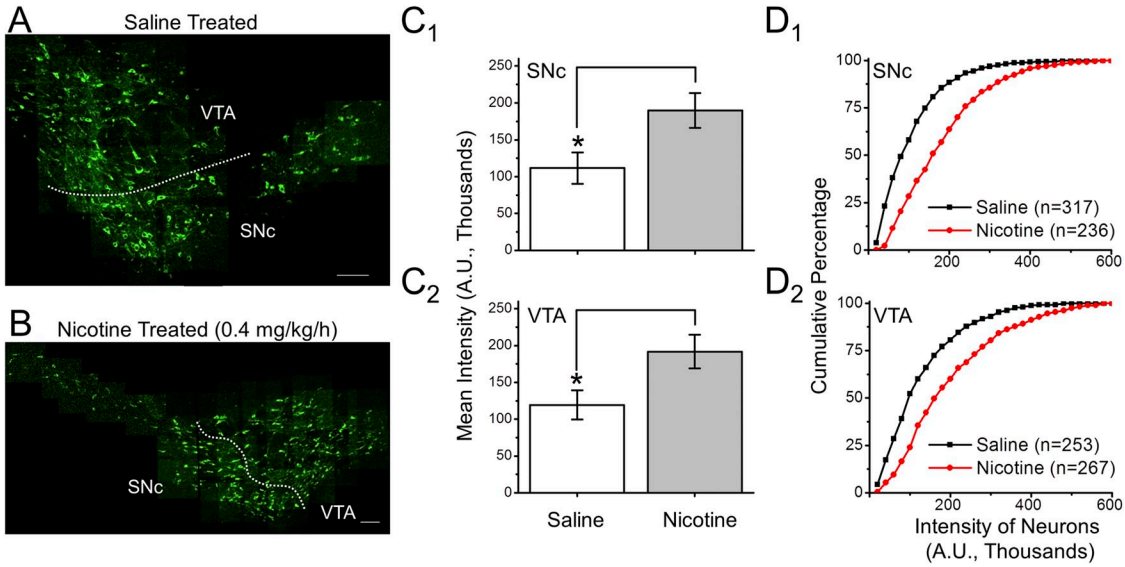

Figure 2. Low concentrations of nicotine (0.4 mg/kg/h) up-regulate α6-GFP* nAChRs in midbrain neurons. (A and B) Direct fluorescence imaging of VTA and SNc neurons in mice expressing α6-GFP subunits after treatment with saline or nicotine (0.4 mg/kg/h, 10 d). Bars, 100 µm. (C_1 and C_2) Quantification of α6-GFP intensities of neurons in saline- or nicotine-treated mice ($n = 4$ mice). (D_1 and D_2) Cumulative percentage plots show changes in α6-GFP fluorescence in the SNc and VTA with chronic nicotine (0.4 mg/kg/h; $n = 4$ mice). *, $P < 0.05$.

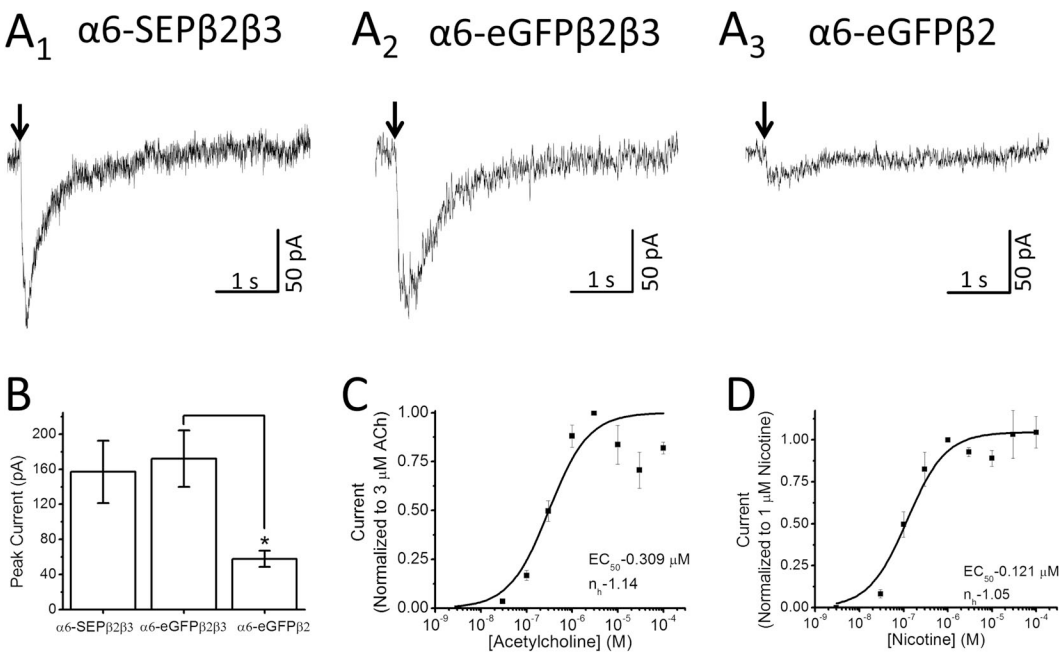

Figure 3. The α6-SEP nAChRs are functional. Representative whole-cell ACh-induced currents of (A_1) α6-SEPβ2β3 nAChRs (3 μM ACh). (A_2) α6-eGFPβ2β3 nAChRs (3 μM ACh) and (A_3) α6-eGFPβ2 nAChRs (300 μM ACh). (B) Comparison of whole-cell ACh-induced current amplitudes of α6-SEPβ2β3, α6-eGFPβ2β3, and α6-eGFPβ2 nAChRs (n = 7–11). (C) Concentration–response of ACh on α6-eGFPβ2β3 nAChRs (n = 15). (D) Concentration-response of (−)-nicotine on α-eGFPβ2β3 nAChRs (n = 14). *, P < 0.05.

Incorporation of β3 subunits increases the density of α6* nAChRs at the PM

We used TIRFM and α6-SEP* nAChRs transfected in Neuro-2A cells to quantify the density of receptors in the peripheral ER versus the PM. Fig. 4 A shows TIRFM images of Neuro-2a cells expressing α6-SEPβ2 or α6-SEPβ2β3 nAChRs at neutral (7.4) and acidic (5.4) pH. As reported previously (Tumkosit et al., 2006), α6β2β3 nAChRs had a higher density on the PM than α6β2 nAChRs; the PMID of α6β2β3 nAChRs was three times that of α6β2 nAChRs (P < 0.0001; Fig. 4 B). We also found a 1.5-fold increase in the PMID of α6β4β3 nAChRs compared with that of α6-SEPβ4* nAChRs (Fig. S1). We found that, when expressed in Neuro-2a

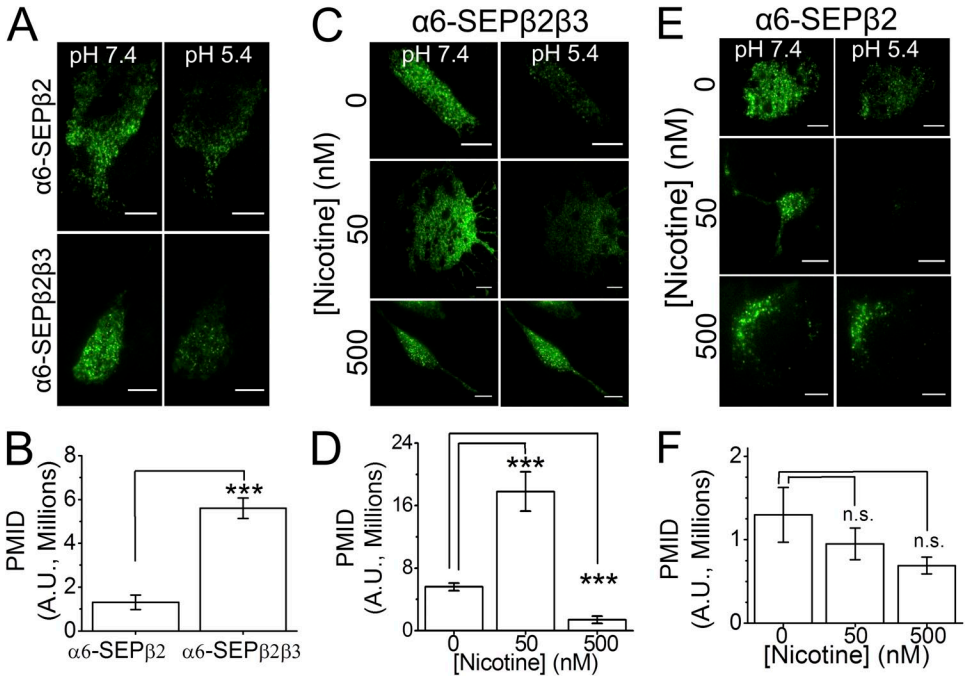

Figure 4. The β3 subunit increases the density of α6* nAChRs at the PM and is necessary for the nicotine-induced up-regulation of α6β2* nAChRs. (A, C, and E) Representative TIRFM images of Neuro-2a cells transfected with α6-SEP and a combination of β2 with or without β3 nAChR subunits at basic (pH 7.4) and acidic (pH 5.4) conditions. Nicotine was added at listed concentrations 24 h before imaging. (B, D, and F) PMID for α6-SEP* nAChRs. Bars, 10 μm (n = 19–23). Data are mean values ± SEM. n.s., not significant; ***, P < 0.0001.

cells, α6-SEPβ3 nAChRs resided almost entirely in the ER (94.5 ± 2.2% ER localization; not depicted). Collectively, these data show that the β3 subunits, combined with β2 or β4 nAChR subunits, increase the density of α6* nAChRs on the PM.

Confirmation that β3 subunits enhance nicotine-induced up-regulation of α6β2* nAChRs

We next assessed the effect of chronic nicotine on α6β2* nAChRs. We examined α6* nAChRs exposed to 50 or 500 nM nicotine for 24 h. 50- and 500-nM nicotine concentrations, respectively, mimic the steady-state and peak concentrations of nicotine found in the brains of smokers (Marks et al., 2004). 50 nM nicotine also equals the plasma concentration produced by 14–21-mg nicotine patches (Schnoll et al., 2013). We observed a significant ($P < 0.0001$) increase in the PMID of α6-SEPβ2β3 nAChRs after treatment with 50 nM nicotine, but a significant ($P < 0.0001$) decrease in PMID after 500-nM nicotine treatment (Fig. 4, C and D). α6-SEPβ2 nAChRs showed no change in PMID after 50-nM nicotine treatment and a decrease in PMID after 500-nM nicotine treatment (Fig. 4, E and F). 50 or 500 nM nicotine induced a greater than threefold increase in α6-SEPβ4* nAChRs PMIDs in the presence or absence of the β3 subunit (Fig. S1).

Dynamic visualization of SEP nAChRs enables us to see when nAChRs arrive at the PM, as they appear as a region of punctate fluorescence (Richards et al., 2011; Fig. 5, A and $B_{1–3}$). We quantified the frequency of these vesicular insertion events at the PM (Fig. 5). After exposure to 50 nM nicotine, we observed a threefold increase in the insertion events of α6-SEPβ2β3 nAChRs ($P < 0.05$) and no change in the insertion events of α6-SEPβ2 nAChRs (Fig. 5, C and D). These data correlated with the observed nicotine-induced changes of PM intensities for α6-SEPβ2β3 and α6-SEPβ2 nAChRs. Specifically, we note a similarity between the increase in PMID and rate of insertion of α6-SEPβ2β3 nAChRs (both are an approximate threefold increase) (Fig. 5, C and D). This suggests that the up-regulation of α6β2β3 nAChRs is caused primarily by increased insertion into the PM, with no major contribution from decreased internalization of receptors from the PM (Lomazzo et al., 2011).

Despite the different PMIDs between α6-SEPβ2β3 and α6-SEPβ2 nAChRs, they showed the same rate of insertion under basal conditions (~12 ins/min). Therefore, the difference in the PM density of α6-SEPβ2β3 and α6-SEPβ2 nAChRs may be caused by differential rates of internalization or stability of these nAChR subtypes at the PM, suggesting that the β3 nAChR subunit may provide a stabilizing effect.

A KKK motif within the β3 M3–M4 loop governs the up-regulation of α6β2β3 nAChRs

Our data suggest that β3 subunits markedly influence the trafficking and dynamics of α6β2* nAChRs. We next sought to identify specific motifs within β3 subunits that may play a role in the trafficking and dynamics of α6β2* nAChRs.

We engineered a series of chimeras: (a) a chimera with a β3 M3–M4 loop replacing the β2 M3–M4 loop in a β2 subunit ($β2_{β3}$) and (b) a chimera with a β2 M3–M4 loop replacing the β3 M3–M4 loop in a β3 subunit ($β3_{β2}$) (see Fig. S2). α6-SEPβ2β2$_{β3}$, α6-SEPβ2$_{β3}$, α6-SEPβ2β3$_{β2}$, and α6-SEPβ3$_{β2}$ nAChRs exhibited typical TIRFM footprints and PM-ER fluorescence that were similar to α6-SEPβ2* nAChRs (Fig. 6). α6-SEPβ2β2$_{β3}$ and α6-SEPβ2$_{β3}$

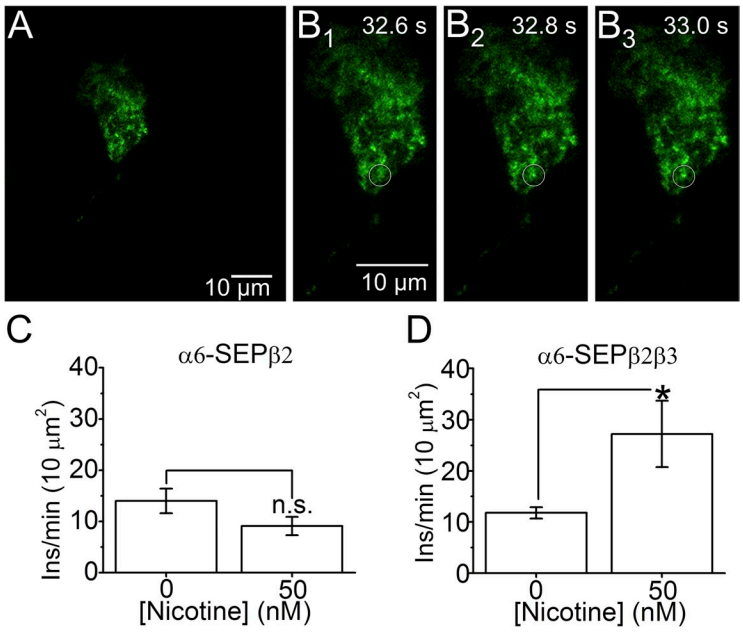

Figure 5. Visualization of membrane insertion events. (A) TIRFM image of a Neuro-2a cell transfected with α6-SEPβ2β3 nAChRs and excited with a 488-nm laser. Images were taken with a frame rate of 200 ms. (B_1) Frame directly preceding an insertion event at the PM. (B_2) Frame showing the insertion and (B_3) the frame directly after the observation of the insertion event. The white circle marks the location of the insertion. (C and D) Frequency of insertion events for α6-SEPβ2* nAChRs without or with nicotine treatment (50 nM, 24 h) calculated as insertion events per minute ($n = 4$). Bars, 10 µm. Data are mean values ± SEM. n.s., not significant; *, $P < 0.05$.

nAChRs up-regulated with 50 nM nicotine, whereas α6-SEPβ3$_{β2}$ and α6-SEPβ2β3$_{β2}$ nAChRs showed either no change or a decrease in the PMID with 50 nM nicotine, suggesting that the β3 subunit M3–M4 domain specifically regulates nicotine-induced up-regulation but may not control the basal trafficking of α6* nAChRs (Fig. 6, A_2 and B_2).

Unique among nAChR subunits, the β3 nAChR subunit possesses a KKK motif within its M3–M4 loop. Dilysine trafficking motifs, including KKxx and KxKxx, facilitate protein binding to COPI, a component of the Golgi–ER retrograde transport machinery (Jackson et al., 2012). Although these motifs typically occur at cytoplasmic C termini, the KKK found in the β3 subunit satisfies both of these consensus motifs. Thus, we hypothesized that the KKK may act as a COPI recognition site. We mutated the ^{381}KKK^{383} motif in the β3 M3–M4 loop to ^{381}AAA^{383} to create β2$_{β3[AAA]}$ and β3$_{AAA}$ nAChR subunits. Mutant nAChRs exhibited a typical TIRFM footprint and showed comparable overall nAChR expression to WT receptors (Fig. 6, C and D). We observed a significant decrease in the number of ER resident α6-SEPβ2β2$_{β3[AAA]}$ and α6-SEPβ2β3$_{AAA}$ nAChRs (Fig. 6, C_1 and D_1). In addition, the α6-SEPβ2β2$_{β3[AAA]}$ and α6-SEPβ2β3$_{AAA}$ nAChRs did not increase the PMID when treated with 50 nM nicotine (Fig. 5, C and D), suggesting that the KKK motif was essential for the nicotine-induced up-regulation of α6-SEPβ2* nAChRs. Similarly, we found a 44% increase in peak ACh-induced currents for α6-eGFPβ2β3 nAChRs after treatment with 50 nM nicotine (24 h) but no increase for α6-eGFPβ2β3$_{AAA}$ nAChRs (Fig. S3). α6-eGFPβ2β3 or α6-eGFPβ2β3$_{AAA}$ nAChRs did not show a difference in ACh-induced currents under basal conditions. These results correlated with the observed PMIDs of α6-SEPβ2β3 and α6-SEPβ2β3$_{AAA}$ nAChRs (Fig. 6).

Nicotine up-regulates nAChRs by binding to and chaperoning ER-localized receptors, which are then trafficked to the PM (Srinivasan et al., 2011). The formation of additional ERES with nicotine is a direct indicator of an event immediately after the nAChR chaperoning process (Srinivasan et al., 2011). To assess the effect of nicotine on α6β2β3$_{AAA}$ nAChR chaperoning, we quantified the formation of condensed ERES (Fig. 7, A and B). Neuro-2a cells were cotransfected with either α6-eGFPβ2β3 or α6-eGFPβ2β3$_{AAA}$ nAChRs and Sec24D-mCherry (a marker for active ERES) (Srinivasan et al., 2011). 50 nM nicotine caused a significant ($P < 0.005$) threefold increase of ERES in α6-eGFPβ2β3 nAChRs but no change in ERES with α6-eGFPβ2β3$_{AAA}$ nAChRs (Fig. 7 B).

The β3 KKK motif inhibits up-regulation by preventing retrograde Golgi to ER nAChR transport

We observed a decrease in the ER density of β3-AAA nAChRs compared with WT nAChRs (Fig. 6, C and D) and hypothesized that loss of the KKK (COPI-binding motif) disrupted trafficking between the Golgi and ER. To test this hypothesis, we studied how WT and β3-AAA nAChRs localized within the Golgi. Fig. 7 (C and D) shows colocalization of α6-eGFPβ2β3 and α6-eGFPβ2β3$_{AAA}$ nAChRs with the Golgi marker GalT-mCherry. β3$_{AAA}$ subunits caused a significant increase in the Pearson

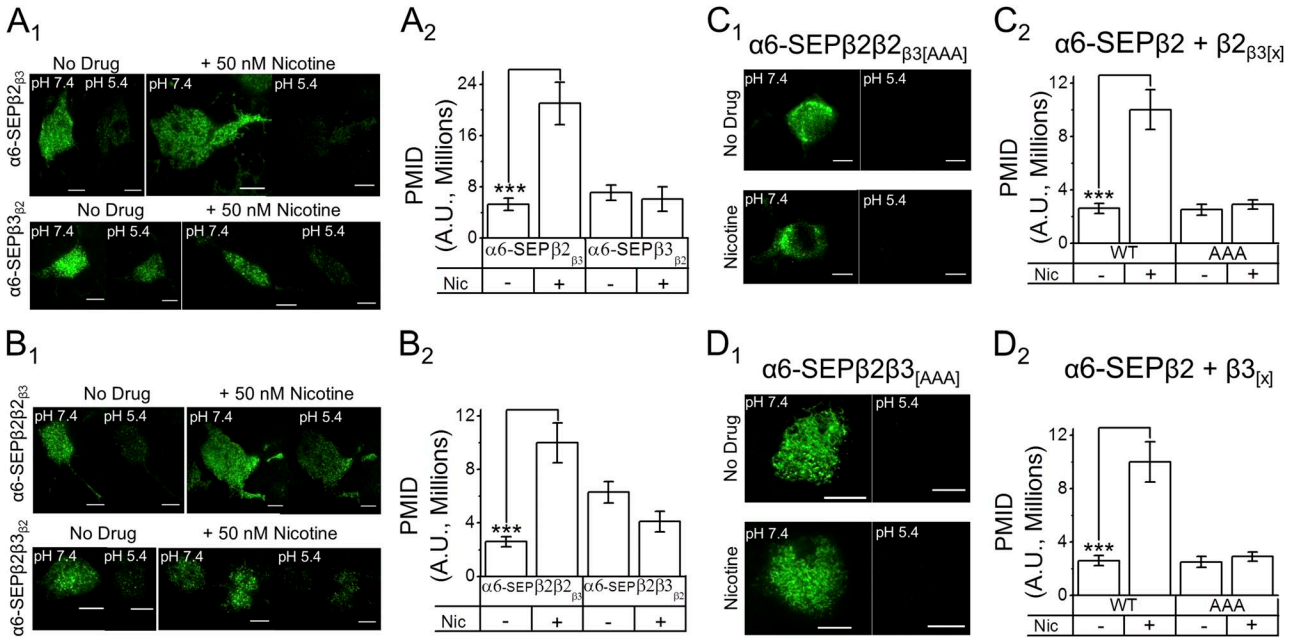

Figure 6. The β3 KKK motif participates in nAChR up-regulation. (A_1, B_1, C_1, and D_1) Representative TIRFM images of Neuro-2a cells transfected with α6-SEP and cotransfected with combinations of β2, β2$_{β3}$, β3$_{β2}$, β2$_{β3[AAA]}$, and β3$_{AAA}$ subunits. 50 nM nicotine was added 24 h after transfection. Bars, 10 µm. (A_2, B_2, C_2, and D_2) PMID for nAChRs (n = 11–27). ***, $P < 0.0001$ (ANOVA).

correlation coefficient for α6-eGFP and GalT-mCherry colocalization (Fig. 7 D_1; $P < 0.0001$) and a significant ($P < 0.01$) increase in the α6-eGFPβ2β3$_{AAA}$ nAChR density when compared with α6-eGFPβ2β3 nAChRs, within the Golgi (Fig. 7 D_2). Therefore, the removal of the KKK motif increased the density of α6β2β3 nAChRs in the Golgi compartment.

To determine whether COPI Golgi–ER trafficking is deficient, we assessed colocalization by immunostaining for endogenous COPI in Neuro-2a cells transfected with α6-eGFPβ2β3 and α6-eGFPβ2β3$_{AAA}$ nAChRs (Fig. 7, E, F_1, and F_2). We found that α6-eGFPβ2β3$_{AAA}$ nAChRs exhibited a significant, twofold decrease in density in COPI vesicles when compared with α6-eGFPβ2β3 nAChRs (Fig. 7 F_1; $P < 0.01$). This was accompanied by a significant decrease in the pixel-based Pearson correlation coefficient among WT and β3-AAA nAChRs ($P < 0.0001$; Fig. 7 F_2). Despite this decrease, we observed no difference in the α6-eGFP* whole-cell fluorescence intensity between α6-eGFPβ2β3 nAChRs and α6-eGFPβ2β3$_{AAA}$ nAChRs (20.2 ± 3.1 and 18.3 ± 4.8 RFUs [millions], respectively). Thus, the potential contribution from degradation is unlikely.

Upon treatment with 50 nM nicotine, we observed a twofold increase in the α6-eGFPβ2β3 nAChR density in COPI vesicles when compared with non-nicotine–treated conditions. In contrast, there was no increase in α6-eGFPβ2β3$_{AAA}$ nAChRs (Fig. 7 F_1). This suggests that after chronic nicotine treatment, an increase of α6* nAChRs in COPI vesicles accompanies the up-regulation observed on the PM. Collectively, these data show that a defect in the recognition between COPI vesicles and α6-eGFPβ2β3$_{AAA}$ nAChRs results in decreased retrograde movement of these nAChRs back into the ER.

The COPI inhibitor CI-976 blocks up-regulation but not basal trafficking of α6β2β3 and α4β2 nAChRs

Our data suggest that Golgi–ER cycling of α6β2β3 nAChRs is necessary for up-regulation during chronic exposure to nicotine. Next, we investigated whether this also applies to other subtypes. For these experiments, we used CI-976, which inhibits COPI-mediated retrograde trafficking at concentrations ≥20 µM (Yang et al., 2005, 2011). Inhibition of COPII vesicle budding occurs at a somewhat higher concentration (50 µM) (Brown et al., 2008).

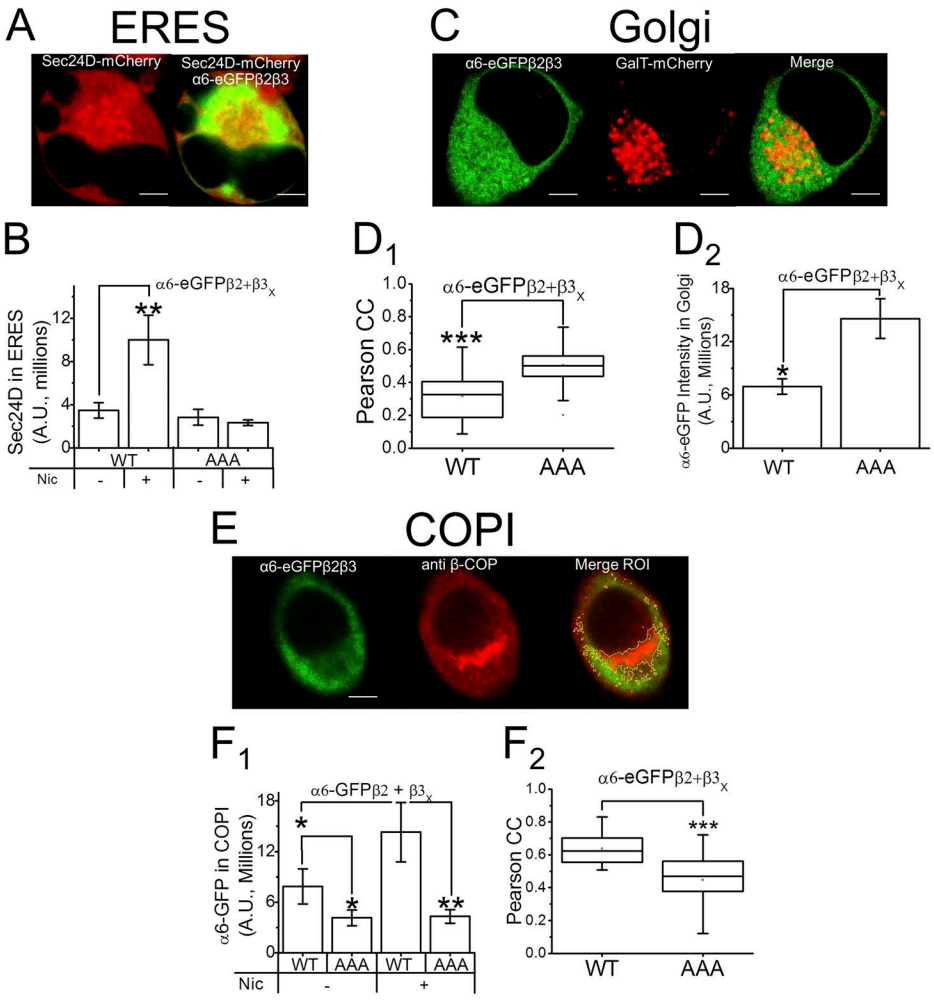

Figure 7. β3-AAA nAChRs show increased density in Golgi despite no change in ER export. Confocal image of α6-eGFPβ2β3 and Sec24D-mCherry (A), α6-eGFPβ2β3 with Golgi marker GalT-mCherry (C), and α6-eGFPβ2β3 nAChRs stained for endogenous β-COP (E). Quantification of: Sec24D fluorescence in ERES per cell for α6-eGFPβ2β3$_{WT}$ and α6-eGFPβ2β3$_{AAA}$ nAChRs (B) ($n = 21–31$); Pearson correlation between α6-eGFP* and GalT-mCherry fluorescence for α6-eGFPβ2β3$_{WT}$ and α6-eGFPβ2β3$_{AAA}$ nAChRs (D_1) ($n = 30–35$); α6-eGFP* intensity in Golgi for α6-eGFPβ2β3$_{WT}$ and α6-eGFPβ2β3$_{AAA}$ nAChRs (D_2) ($n = 30–35$); α6-eGFP fluorescence in COPI vesicles for α6-eGFPβ2β3$_{WT}$ and α6-eGFPβ2β3$_{AAA}$ nAChRs (F_1) ($n = 23–25$); and Pearson correlation for the colocalization of α6-eGFP* fluorescence with COPI fluorescence in α6-eGFPβ2β3$_{WT}$ and α6-eGFPβ2β3$_{AAA}$ nAChRs (F_2) ($n = 23–24$). Bars, 5 µm. *, $P < 0.01$; **, $P < 0.005$; ***, $P < 0.0001$ (ANOVA).

First, we assessed the effects of 20 µM CI-976 on ERES (Fig. S4 A). CI-976 did not affect the basal number of ERES in α6-GFPβ2β3 nAChRs but did prevent the increase in ERES with chronic nicotine treatment (50 nM). This is the same trend that was observed with α6-GFPβ2β3$_{AAA}$ nAChRs (see Fig. 6 D_2). With CI-976 treatment, we also noted a significant ($P < 0.005$) increase in the α6-GFP density in the Golgi (Fig. S4 B) and a significant ($P < 0.05$) increase in the Pearson correlation coefficient for colocalization of α6-eGFP and GalT-mCherry (Fig. S4 C). These data mimic the results seen with α6-GFPβ2β3$_{AAA}$ nAChRs (Fig. 7) and suggest that CI-976 can be used to study the inhibition of Golgi–ER cycling in nAChRs.

COPI may play a role in anterograde transport in addition to its role in retrograde transport (Yang et al., 2011). We conducted experiments to determine whether the concentration of CI-976 we used inhibited COPI-mediated anterograde traffic of nAChRs. We studied α4β4 and α4β2$_{enhanced\text{-}ER\text{-}export}$ (also called α4β2-DM nAChRs), which both have a high rate of passage from ER to the PM (Richards et al., 2011; Srinivasan et al., 2011). We reasoned that if CI-976 reduced the PMID of either α4β4 or α4β2-DM nAChRs, it would indicate an inhibitory effect on COPI-mediated anterograde traffic. We observed no change in the PMID of α4β4 or α4β2-DM nAChRs after CI-976 treatment (Fig. S5). We also note (again) that COPI did not change the level of basal ERES (Fig. S4 A), arguing against the idea that exit from the ER is affected by CI-976. Collectively, these data suggest that CI-976 effects are exerted on COPI's retrograde pathway only.

α6β2β3 nAChRs treated with CI-976 produced similar trends compared to α6β2β3$_{AAA}$ nAChRs (compare Figs. 6 D_2 to 8 B_1). As usual, 50 nM nicotine treatment produced a significant ($P < 0.005$) increase in the PMID of α6-SEPβ2β3 nAChRs (Fig. 8 B_1). Treatment with 20 µM CI-976 alone did not differ from the basal conditions seen in α6-SEPβ2β3 nAChRs (no change in PMID), but when cells were coexposed to CI-976 and nicotine, up-regulation of α6-SEPβ2β3 nAChRs was blocked (Fig. 8 B_1). Previous analyses show that 100 nM nicotine is an appropriate concentration for the study of α4-SEPβ2 nAChR up-regulation (Richards et al., 2011; Srinivasan et al., 2011). We observed a significant ($P < 0.05$) increase in the α4-SEPβ2 nAChR PMID with

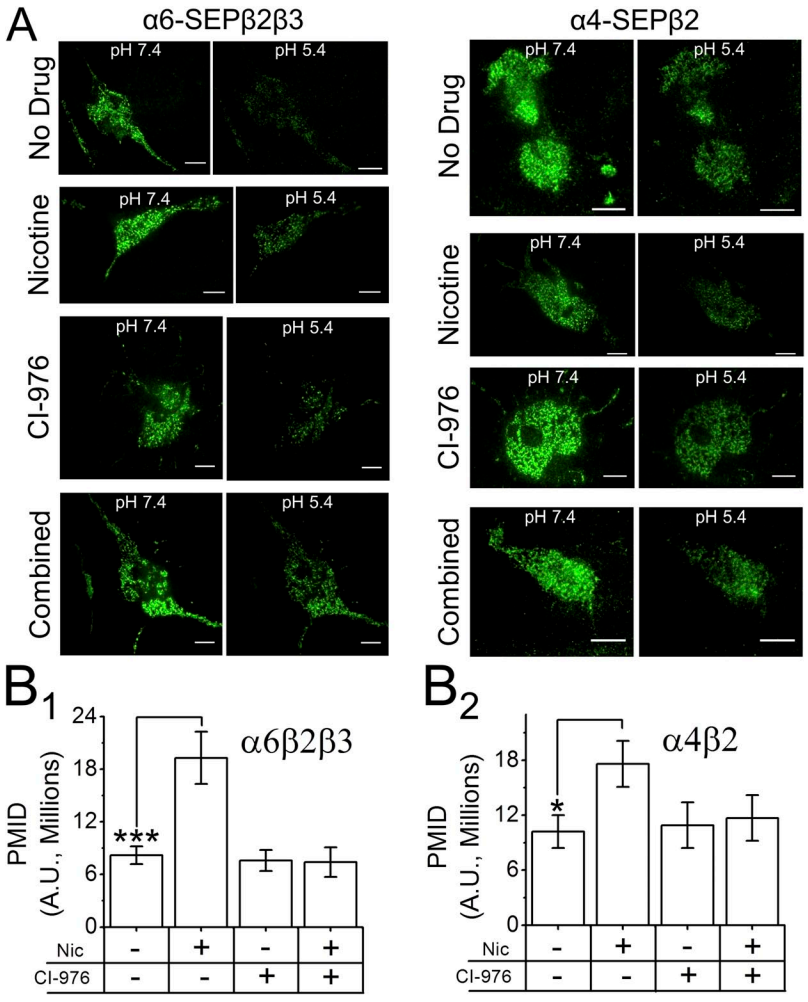

Figure 8. Blocking Golgi–ER cycling prevents up-regulation of nAChRs. (A) Representative TIRFM images of α4-SEPβ2 (right) or α6-SEPβ2β3 (left) nAChR subunits. Nicotine (50 nM α6-SEPβ2β3 nAChRs or 100 nM α4-SEPβ2 nAChRs) and/or 20 µM CI-796 were added 24 h before imaging. Bars, 10 µm. Quantification of PMID for α6-SEPβ2β3 nAChRs (B_1) or α4-SEPβ2 nAChRs (B_2) in Neuro-2a cells with drug treatments: no drug, nicotine, CI-976, or combined (n = 17–23). *, $P < 0.05$; ***, $P < 0.0001$ (ANOVA).

100 nM nicotine and, similar to our observations in α6-SEPβ2β3 nAChRs, treatment of α4-SEPβ2 nAChRs with CI-976 alone did not differ from basal conditions (no change in PMID) (Fig. 8 B_2). When both CI-976 and nicotine were present with α4-SEPβ2 nAChRs, up-regulation was prevented (Fig. 8 B_2). These results suggest that a COPI-dependent process, related to Golgi–ER cycling, is necessary for the nicotine-induced up-regulation of α4β2 as well as α6β2β3 nAChRs.

NFRET measurements of the α6β2β3–εCOP interaction

We asked whether nAChRs and COPI display NFRET. Neuro-2a cells were transfected with α6-mCherry, β2, and β3 (WT and β3-AAA) nAChR subunits along with εCOP-eGFP (Fig. 9 A). Fig. 9 A shows that NFRET between α6-mCherry and εCOP-eGFP exhibited patterns similar to endogenous βCOP staining (see Fig. 7 E). Evidently, α6-mCherry and εCOP-eGFP colocalize within ∼100 Å.

We asked whether the β3-AAA mutation or CI-976 can inhibit the interaction between α6β2β3 and εCOP. nAChRs with the β3-AAA mutation consistently shifted pixel-based NFRET amplitude distributions to lower values (Fig. 9, A–C). Treatment with CI-976 also consistently shifted pixel-based NFRET amplitude distributions to lower values (Fig. 9, A–C). Similarly, when we assigned an NFRET value to each cell by calculating the average NFRET of the cell's nonzero FRET pixels, the NFRET among cells was significantly decreased in the presence of nAChRs with the β3-AAA mutation or treatment with CI-976 (Fig. 9 C). In addition to NFRET, we used εCOP-GFP fluorescence to demarcate ROI for COPI vesicles, and then examined the density of α6* nAChRs in the COPI ROI (as in Fig. 7 F_1). α6-eGFPβ2β3$_{AAA}$ nAChRs (no drug) and WT α6-eGFPβ2β3 nAChRs (treated with CI-976) exhibited a significant decrease in their density within COPI vesicles (Fig. 9 D; $P < 0.005$). This was accompanied by a significant decrease in the pixel-based Pearson correlation coefficient (Fig. 9 E). Collectively, these results demonstrate that disruption of the KKK motif or inhibition of COPI destabilizes the interaction between COPI and α6β2β3 nAChRs.

DISCUSSION

α6* nAChRs up-regulate after chronic nicotine treatment

This paper documents the in vivo up-regulation of α6* nAChR protein at a sustained nicotine concentration comparable to that in human smokers. We found that up-regulation occurs in the four major brain regions that express α6-GFP nAChRs: VTA, SNc, medial habenula, and superior colliculus (see Figs. 1 and 2).

The α6 and β3 nAChR subunits have nearly identical expression patterns in the brain, as reported by analysis

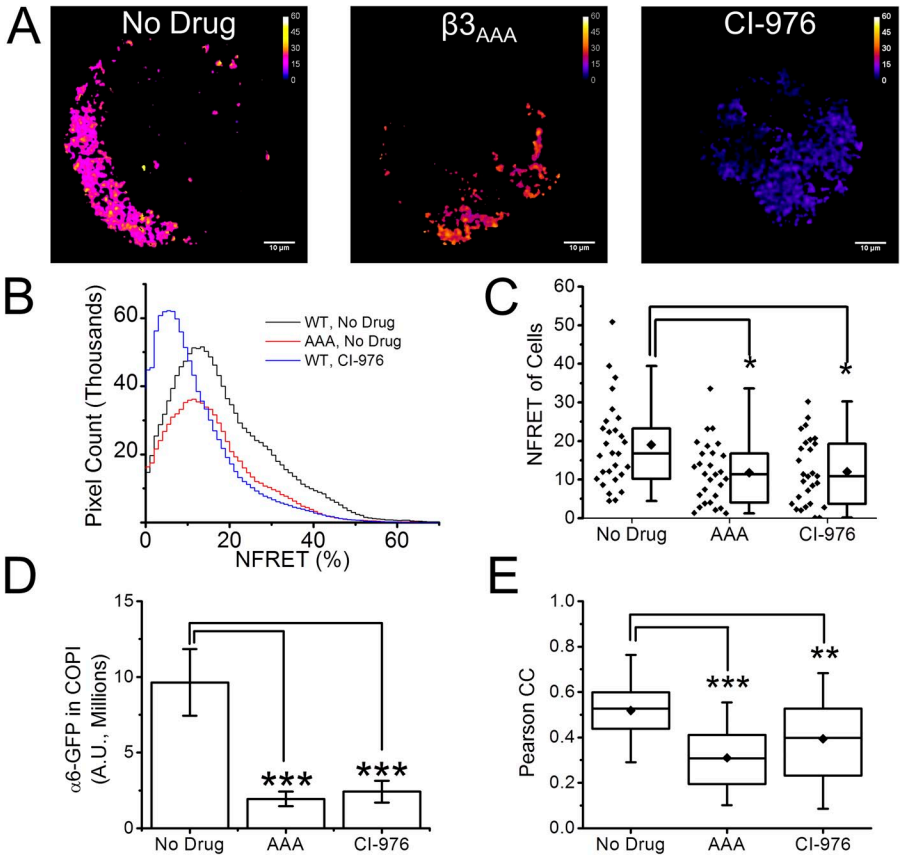

Figure 9. β3-AAA nAChRs and CI-976 treatment decrease interaction between α6 and COPI. NFRET measurements were made using α6-mCherry and εCOP-eGFP transfected in Neuro-2a cells (along with β2 and β3wt or β3$_{AAA}$ subunits). (A) Representative NFRET images between α6-mCherry and εCOP-eGFP in Neuro-2a cells. Bars, 10 µm. (B) Summed histograms of pixel-based NFRET measurements, representative of four independent NFRET assays ($n = 20$ cells). C–E show analysis of the same group of cells ($n = 28$ cells). (C) Another of the four experiments. Scatter-box plot for the mean NFRET values of individual cells. The larger black diamond (◆) in the box plot represents the cell-based mean of each condition. (D) α6-eGFP fluorescence in COPI vesicles for α6-eGFPβ2β3$_{AAA}$ nAChRs and α6-eGFPβ2β3$_{WT}$ nAChRs (without and with 20 µM CI-976). (E) Pearson correlation for the colocalization of α6-eGFP* fluorescence with εCOP-GFP fluorescence ($n = 28$ cells). *, $P < 0.05$; **, $P < 0.01$; ***, $P < 0.005$ (ANOVA).

of mRNA and autoradiography (Le Novère et al., 1996; Azam et al., 2002; Baddick and Marks, 2011). In heterologous systems, α6β2β3 nAChRs show better function (higher density on the PM, larger peak current response) than α6β2. Therefore, it is appropriate to study effects of chronic nicotine on α6β2* nAChRs in the context of coexpressed β3 subunits. We found that, at concentrations mimicking the steady-state levels found in human smokers and during nicotine replacement therapy (50 nM nicotine), α6-SEPβ2β3 nAChRs up-regulate whereas α6-SEPβ2 nAChRs failed to up-regulate. The β3 subunit thus appears necessary for the up-regulation of α6-SEPβ2* nAChRs. This agrees well with Tumkosit et al. (2006), who showed that β3 nAChR subunits promote nicotine-induced up-regulation of α6* nAChRs.

Our observations of α6* up-regulation agree with some previously published work (Parker et al., 2004; Perez et al., 2008; Walsh et al., 2008). Other studies found that chronic nicotine treatment leads to a decrease in the contribution of α6* nAChRs, as identified by binding or dopamine release assays (Lai et al., 2005; Perry et al., 2007; Exley et al., 2013). Several factors may contribute to these disparate findings. First, the up-regulation of α6* nAChRs we observed was in midbrain (VTA and SNc) dopaminergic neurons, whereas the studies showing a decrease in α6* nAChR contribution were completed in the striatal regions. We have confirmed previously that α6-GFP* nAChRs in the VTA and SNc are localized exclusively in dopaminergic neurons (Mackey et al., 2012). The difference in striatal (down-regulation) and midbrain (up-regulation) may be explained by a different population of nAChRs (α6α4*, α6[nonα4]*, α6β3*, and/or α6[nonβ3]*). Perez et al. (2008) have shown that although α6(nonα4)* nAChRs up-regulate, α6α4* nAChRs down-regulate. We, along with others (Tumkosit et al., 2006), have shown that α6* nAChRs may require the β3 subunit to up-regulate. Therefore, the population of nAChRs residing in the somata of midbrain dopaminergic neurons may be composed of

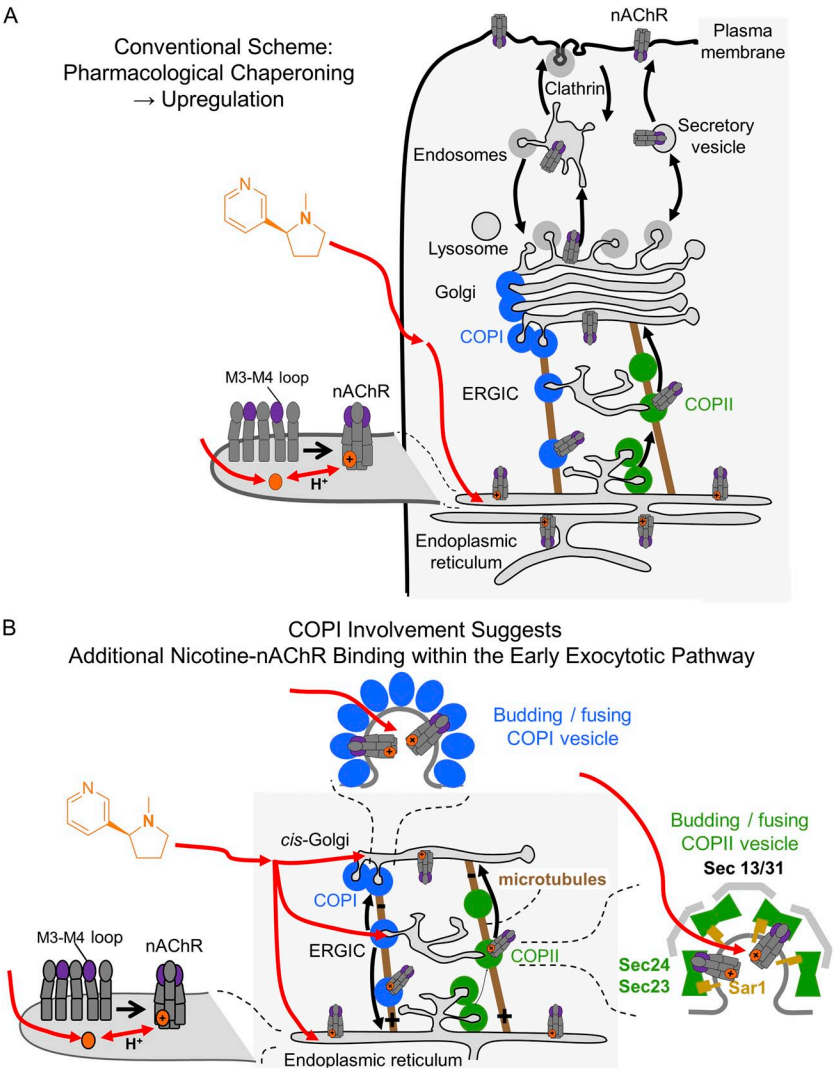

Figure 10. A schematic representation of selective pharmacological chaperoning of nAChRs in response to chronic nicotine. (A) Nicotine interconverts within milliseconds between the protonated membrane-impermeant form and the neutral membrane-permeant form. The latter enters cells and enters the ER (red arrow). Here, the charged form pharmacologically chaperones nAChRs so that increased numbers exit toward the Golgi via the COPII pathway, eventually resulting in receptor up-regulation at the PM. Thus, pharmacological chaperoning by nicotine is thought to underlie the process of nAChR up-regulation by chronic nicotine. (B) This study finds that nicotine-mediated up-regulation also depends on the COPI machinery involved in ER to Golgi and Golgi to ER transport of nAChRs. One possible explanation for the COPI dependence is that nicotine enters additional organelles and binds more extensively than previously thought within the early exocytic pathway, shown by the additional red arrows leading to both COPI and COPII vesicles, ERGIC, and cis-Golgi. See also the animation, "Nicotine Up-regulates nAChRs": http://www.jgp.org/cgi/content/full/jgp.201311102/DC2.

more α6(nonα4)β3* nAChRs than α6α4* or α6(nonβ3)* nAChRs. However, there may be more α6α4* or α6(nonβ3)* nAChRs on these neurons' dopaminergic terminals in the striatum and accumbens. This is supported by a report that there are more α6α4* nAChRs on dopaminergic terminals (in striatum and accumbens) than there are on dopaminergic cell bodies (in VTA and SNc) (Champtiaux et al., 2003).

Second, differing concentrations of nicotine were used in the different studies. The doses of nicotine we used in mice (2 mg/kg/h and 0.4 mg/kg/h) produce plasma concentrations of <500 and <100 nM nicotine, respectively (Marks et al., 2004). Perry et al. (2007) used a dose (6 mg/kg/day) in rats that produces >500 nM plasma nicotine (Nguyen et al., 2004). Our data show that 500 nM nicotine decreased the density of α6* nAChRs on the PM (Fig. 4, D and F). Therefore, the differences observed in our current work and in that of others (Lai et al., 2005; Perry et al., 2007; Exley et al., 2013) may be caused by the concentration of nicotine used.

The KKK motif of β3 nAChR subunit suggests that a COPI-mediated retrograde pathway participates in up-regulation

A KKK motif appears in the M3–M4 intracellular loop of the β3 nAChR subunit. COPI binds to di-lysine motifs (KKxx or KxKxx) (Jackson et al., 2012; Ma and Goldberg, 2013), and the KKK of the β3 subunit satisfies both motifs. Measurements of FRET between α6β2β3 nAChRs and εCOP indicate that the two molecules approach with ∼100 Å, and this interaction is decreased by mutating the β3-KKK sequence to β3-AAA (Fig. 9). This suggests that one of these di-lysine motifs in β3 mediates a direct interaction between nAChRs and COPI.

We hypothesized that COPI likely plays a role in the retrograde transport of α6β2β3 nAChRs from the Golgi back to the ER. α6* nAChRs with a β3-AAA in place of β3-KKK failed to up-regulate on the PM in the presence of nicotine. We found that the ER localization of the α6-SEPβ2β3$_{AAA}$ nAChRs was decreased compared with α6-SEPβ2β3 nAChRs, suggesting that the β3-AAA motif changed the distribution of nAChRs among organelles in the early secretory pathway. Indeed, we found that the α6-SEPβ2β3$_{AAA}$ nAChRs had a significantly higher localization within the Golgi than the α6-SEPβ2β3 nAChRs (Fig. 7, C, D_1, and D_2).

When we add the fact that the number of ERES does not differ between the α6β2β3 and α6β2β3$_{AAA}$ nAChRs in basal conditions (e.g., no nicotine) (Fig. 7, A and B), we can conclude that the export (via COPII vesicles) of nAChRs is not affected. Thus, α6β2β3$_{AAA}$ nAChRs are exported from the ER at a rate similar to that of α6β2β3 nAChRs. Because export (COPII mediated) is not affected, this suggests that retrieval (COPI mediated) is responsible for the disrupted trafficking. This was confirmed when we observed significantly fewer α6β2β3$_{AAA}$ nAChRs in COPI vesicles when compared with α6β2β3 nAChRs (see Fig. 7, E, F_1, and F_2). Furthermore, β3-AAA nAChRs shifted the NFRET distribution to lower values compared with WT nAChRs (see Fig. 9). Collectively, these data suggest that the disruption of the KKK motif results in deficient retrograde transport of nAChRs between the Golgi and ER. Although one cannot draw specific conclusions about the locus of interference in the cyclic processes involving ER, COPII, cis-Golgi, and COPI (Orci et al., 1997), the data suggest that this disrupted cycling from the Golgi back to the ER prevents up-regulation during exposure to nicotine.

A COPI-dependent process, such as Golgi–ER cycling, is necessary for the up-regulation of nAChRs

We asked whether Golgi–ER cycling plays a role in the other case of nAChRs (α4β2) that up-regulate at smoking-relevant concentrations of nicotine. Because the β3 KKK motif is unique in nAChR subunits, we exploited a more general inhibitor approach, CI-976, to block COPI function. On α6β2β3 nAChRs, CI-976 produced results that resembled the pattern observed for β3-WT and β3-AAA nAChRs (compare Figs. 8 B_1 with 6 D_2). Inhibiting Golgi–ER cycling prevented up-regulation of α6β2β3 and α4β2 nAChRs after nicotine treatment. This suggests that the cycling of nAChRs between the Golgi and ER is necessary for the up-regulation of nAChRs on the PM.

Previous reports indicate that nAChR up-regulation is initiated within intracellular compartments and that the locus is partially in the ER (see Fig. 10) (Kuryatov et al., 2005; Sallette et al., 2005; Lester et al., 2009; Miwa et al., 2011; Srinivasan et al., 2011). The data presented here suggest novel aspects of the up-regulation of nAChRs, related to general observations that secretory pathways have both regulated and constitutive components. The increased nAChR density on the PM results from increased ER export of α6β2β3 nAChRs (increase in ERES/COPII, leading to increased insertion events). Previous data show that this also occurs in α4β2 nAChRs (Richards et al., 2011; Srinivasan et al., 2011) (depicted in Fig. 10). We show here that chronic nicotine also increases the number of nAChRs in COPI vesicles (Fig. 7 F_1). This suggests that in addition to an increase in ER export, there is also an increase of retrograde movement of nAChRs from the Golgi to the ER. Possibly, α6β2β3 and α4β2 nAChRs are continually cycled between the ER and Golgi through COPI and COPII. This cycling maintains a population of nAChRs in the ER that may be necessary for up-regulation. In the absence of nicotine, disruption of Golgi–ER cycling (either through the β3-AAA mutants or use of CI-976) does not affect PM nAChR density (Figs. 8 B_1 and 6 D_2). However, when Golgi–ER cycling is inhibited and nicotine is present, nicotine cannot produce up-regulated PM nAChRs.

How does nicotine exploit a COPI process to up-regulate PM nAChRs? There are three nonmutually exclusive possibilities. (1) Decreased retrieval of nAChRs

from the Golgi produces an increased number of Golgi-resident nAChRs but a reduced number of ER-resident nAChRs. Individual nAChRs therefore spend a smaller fraction of time in the ER. Perhaps this renders them less available for pharmacological chaperoning by nicotine (Fig. 10 A). Such chaperoning seems to be relatively inefficient, even though it takes place at nicotine concentrations 10–100 times lower than that required for activation of PM nAChRs. This inefficiency could occur because binding of nicotine must await the dissociation of a competing endogenous chaperone protein such as lynx1 (Miwa et al., 2012). (2) Pharmacological chaperoning by nicotine does stabilize pentameric nAChRs in the ER (Whiteaker et al., 1998; Sallette et al., 2005) but is nonetheless a pathological process that could block or prevent one or more modifications required for efficient exit from the Golgi to the PM. If the nAChRs chaperoned by nicotine fail to pass the quality control checks in the Golgi, they would be targeted for retrieval back to the ER via a COPI-dependent process. (3) An intriguing possibility is that nicotine may enter additional organelles within the early exocytotic pathway. Nicotine might remain bound to nAChRs while the nAChRs reside in COPI and/or COPII vesicles (Fig. 10 B). Processes related to pharmacological chaperoning, termed "matchmaking," "escorting," or "abduction," might occur in these vesicles (Lester et al., 2012). Because the ER and cis-Golgi have nearly neutral lumenal pH, acid trapping of nicotine (Jia et al., 2003; Lester et al., 2009) probably plays little role in the processes studied here.

Golgi–ER cycling as a new mechanistic target for drug discovery

Discovery of the role played by Golgi–ER cycling in both α6β2β3 and α4β2 nAChRs may eventually provide additional avenues for nicotine addiction therapies. A hypothetical small molecule designed to bind to the KKK and disrupt COPI binding would prevent the Golgi–ER cycling in a manner similar to observations in this work. This inhibition of Golgi–ER cycling would prevent the up-regulation of β3-containing nAChRs and may produce effects similar to many antagonists that have shown clinical promise (Watkins et al., 1999; Rauhut et al., 2003; Yoshimura et al., 2007). In the search for potential therapeutics, the selective expression pattern of α6β2β3 nAChRs to just a few neuronal populations would render the targeting of β3 more selective than a drug that inhibits Golgi–ER cycling in general.

We thank Jennifer Lippincott-Schwartz for kindly providing εCOP-GFP subunits for our studies, Rell Parker for comments, and the Barbara Wold laboratory for providing cryosectioning tools.

This work was supported by National Institutes of Health (grants AG033954, DA017279, DA019375, DA030396, NS034407, and DA033721) and by the California Tobacco-Related Disease Research Program (grant 17RT0127). Louis and Janet Fletcher provided partial funding for the TIRF microscope.

The authors have no conflicting financial interests.

Edward N. Pugh Jr. served as editor.

Submitted: 16 September 2013
Accepted: 6 December 2013

REFERENCES

Araki, Y., D.T. Lin, and R.L. Huganir. 2010. Plasma membrane insertion of the AMPA receptor GluA2 subunit is regulated by NSF binding and Q/R editing of the ion pore. *Proc. Natl. Acad. Sci. USA.* 107:11080–11085. http://dx.doi.org/10.1073/pnas.1006584107

Asokan, A., and M.J. Cho. 2002. Exploitation of intracellular pH gradients in the cellular delivery of macromolecules. *J. Pharm. Sci.* 91:903–913. http://dx.doi.org/10.1002/jps.10095

Azam, L., U.H. Winzer-Serhan, Y. Chen, and F.M. Leslie. 2002. Expression of neuronal nicotinic acetylcholine receptor subunit mRNAs within midbrain dopamine neurons. *J. Comp. Neurol.* 444:260–274. http://dx.doi.org/10.1002/cne.10138

Baddick, C.G., and M.J. Marks. 2011. An autoradiographic survey of mouse brain nicotinic acetylcholine receptors defined by null mutants. *Biochem. Pharmacol.* 82:828–841. http://dx.doi.org/10.1016/j.bcp.2011.04.019

Benwell, M.E., D.J. Balfour, and J.M. Anderson. 1988. Evidence that tobacco smoking increases the density of (−)-[^{3}H]nicotine binding sites in human brain. *J. Neurochem.* 50:1243–1247. http://dx.doi.org/10.1111/j.1471-4159.1988.tb10600.x

Brandizzi, F., and C. Barlowe. 2013. Organization of the ER-Golgi interface for membrane traffic control. *Nat. Rev. Mol. Cell Biol.* 14:382–392. http://dx.doi.org/10.1038/nrm3588

Breese, C.R., M.J. Marks, J. Logel, C.E. Adams, B. Sullivan, A.C. Collins, and S. Leonard. 1997. Effect of smoking history on [^{3}H]nicotine binding in human postmortem brain. *J. Pharmacol. Exp. Ther.* 282:7–13.

Brown, W.J., H. Plutner, D. Drecktrah, B.L. Judson, and W.E. Balch. 2008. The lysophospholipid acyltransferase antagonist CI-976 inhibits a late step in COPII vesicle budding. *Traffic.* 9:786–797. http://dx.doi.org/10.1111/j.1600-0854.2008.00711.x

Brunzell, D.H., K.E. Boschen, E.S. Hendrick, P.M. Beardsley, and J.M. McIntosh. 2010. α-conotoxin MII-sensitive nicotinic acetylcholine receptors in the nucleus accumbens shell regulate progressive ratio responding maintained by nicotine. *Neuropsychopharmacology.* 35:665–673. http://dx.doi.org/10.1038/npp.2009.171

Champtiaux, N., C. Gotti, M. Cordero-Erausquin, D.J. David, C. Przybylski, C. Léna, F. Clementi, M. Moretti, F.M. Rossi, N. Le Novère, et al. 2003. Subunit composition of functional nicotinic receptors in dopaminergic neurons investigated with knock-out mice. *J. Neurosci.* 23:7820–7829.

Drenan, R.M., R. Nashmi, P.I. Imoukhuede, H. Just, S. McKinney, and H.A. Lester. 2008. Subcellular trafficking, pentameric assembly, and subunit stoichiometry of neuronal nicotinic acetylcholine receptors containing fluorescently labeled α6 and β3 subunits. *Mol. Pharmacol.* 73:27–41. http://dx.doi.org/10.1124/mol.107.039180

Exley, R., M.A. Clements, H. Hartung, J.M. McIntosh, M. Franklin, I. Bermudez, and S.J. Cragg. 2013. Striatal dopamine transmission is reduced after chronic nicotine with a decrease in α6-nicotinic receptor control in nucleus accumbens. *Eur. J. Neurosci.* 38:3036–3043. http://dx.doi.org/10.1111/ejn.12298.

Flores, C.M., S.W. Rogers, L.A. Pabreza, B.B. Wolfe, and K.J. Kellar. 1992. A subtype of nicotinic cholinergic receptor in rat brain is composed of α4 and β2 subunits and is up-regulated by chronic nicotine treatment. *Mol. Pharmacol.* 41:31–37.

Jackson, K.J., J.M. McIntosh, D.H. Brunzell, S.S. Sanjakdar, and M.I. Damaj. 2009. The role of alpha6-containing nicotinic acetylcholine receptors in nicotine reward and withdrawal. *J. Pharmacol. Exp. Ther.* 331:547–554. http://dx.doi.org/10.1124/jpet.109.155457

Jackson, L.P., M. Lewis, H.M. Kent, M.A. Edeling, P.R. Evans, R. Duden, and D.J. Owen. 2012. Molecular basis for recognition of dilysine trafficking motifs by COPI. *Dev. Cell.* 23:1255–1262. http://dx.doi.org/10.1016/j.devcel.2012.10.017

Jacob, T.C., Y.D. Bogdanov, C. Magnus, R.S. Saliba, J.T. Kittler, P.G. Haydon, and S.J. Moss. 2005. Gephyrin regulates the cell surface dynamics of synaptic $GABA_A$ receptors. *J. Neurosci.* 25:10469–10478. http://dx.doi.org/10.1523/JNEUROSCI.2267-05.2005

Jaskolski, F., B. Mayo-Martin, D. Jane, and J.M. Henley. 2009. Dynamin-dependent membrane drift recruits AMPA receptors to dendritic spines. *J. Biol. Chem.* 284:12491–12503. http://dx.doi.org/10.1074/jbc.M808401200

Jia, L., K. Flotildes, M. Li, and B.N. Cohen. 2003. Nicotine trapping causes the persistent desensitization of α4β2 nicotinic receptors expressed in oocytes. *J. Neurochem.* 84:753–766. http://dx.doi.org/10.1046/j.1471-4159.2003.01578.x

Koob, G.F. 2009. New dimensions in human laboratory models of addiction. *Addict. Biol.* 14:1–8. http://dx.doi.org/10.1111/j.1369-1600.2008.00127.x

Kuryatov, A., and J. Lindstrom. 2011. Expression of functional human α6β2β3* acetylcholine receptors in *Xenopus laevis* oocytes achieved through subunit chimeras and concatamers. *Mol. Pharmacol.* 79:126–140. http://dx.doi.org/10.1124/mol.110.066159

Kuryatov, A., J. Luo, J. Cooper, and J. Lindstrom. 2005. Nicotine acts as a pharmacological chaperone to up-regulate human α4β2 acetylcholine receptors. *Mol. Pharmacol.* 68:1839–1851.

Lai, A., N. Parameswaran, M. Khwaja, P. Whiteaker, J.M. Lindstrom, H. Fan, J.M. McIntosh, S.R. Grady, and M. Quik. 2005. Long-term nicotine treatment decreases striatal α6* nicotinic acetylcholine receptor sites and function in mice. *Mol. Pharmacol.* 67:1639–1647. http://dx.doi.org/10.1124/mol.104.006429

Le Novère, N., M. Zoli, and J.P. Changeux. 1996. Neuronal nicotinic receptor α6 subunit mRNA is selectively concentrated in catecholaminergic nuclei of the rat brain. *Eur. J. Neurosci.* 8:2428–2439. http://dx.doi.org/10.1111/j.1460-9568.1996.tb01206.x

Lester, H.A., C. Xiao, R. Srinivasan, C.D. Son, J. Miwa, R. Pantoja, M.R. Banghart, D.A. Dougherty, A.M. Goate, and J.C. Wang. 2009. Nicotine is a selective pharmacological chaperone of acetylcholine receptor number and stoichiometry. Implications for drug discovery. *AAPS J.* 11:167–177. http://dx.doi.org/10.1208/s12248-009-9090-7

Lester, H.A., J.M. Miwa, and R. Srinivasan. 2012. Psychiatric drugs bind to classical targets within early exocytotic pathways: therapeutic effects. *Biol. Psychiatry.* 72:907–915. http://dx.doi.org/10.1016/j.biopsych.2012.05.020

Lin, D.T., Y. Makino, K. Sharma, T. Hayashi, R. Neve, K. Takamiya, and R.L. Huganir. 2009. Regulation of AMPA receptor extrasynaptic insertion by 4.1N, phosphorylation and palmitoylation. *Nat. Neurosci.* 12:879–887. http://dx.doi.org/10.1038/nn.2351

Lomazzo, E., G.P. Hussmann, B.B. Wolfe, R.P. Yasuda, D.C. Perry, and K.J. Kellar. 2011. Effects of chronic nicotine on heteromeric neuronal nicotinic receptors in rat primary cultured neurons. *J. Neurochem.* 119:153–164. http://dx.doi.org/10.1111/j.1471-4159.2011.07408.x

Ma, W., and J. Goldberg. 2013. Rules for the recognition of dilysine retrieval motifs by coatomer. *EMBO J.* 32:926–937. http://dx.doi.org/10.1038/emboj.2013.41

Mackey, E.D., S.E. Engle, M.R. Kim, H.C. O'Neill, C.R. Wageman, N.E. Patzlaff, Y. Wang, S.R. Grady, J.M. McIntosh, M.J. Marks, et al. 2012. α6* nicotinic acetylcholine receptor expression and function in a visual salience circuit. *J. Neurosci.* 32:10226–10237. http://dx.doi.org/10.1523/JNEUROSCI.0007-12.2012

Mamede, M., K. Ishizu, M. Ueda, T. Mukai, Y. Iida, H. Kawashima, H. Fukuyama, K. Togashi, and H. Saji. 2007. Temporal change in human nicotinic acetylcholine receptor after smoking cessation: 5IASPECT study. *J. Nucl. Med.* 48:1829–1835. http://dx.doi.org/10.2967/jnumed.107.043471

Mani, M., and T.A. Ryan. 2009. Live imaging of synaptic vesicle release and retrieval in dopaminergic neurons. *Front Neural Circuits.* 3:3.

Marks, M.J., J.B. Burch, and A.C. Collins. 1983. Effects of chronic nicotine infusion on tolerance development and nicotinic receptors. *J. Pharmacol. Exp. Ther.* 226:817–825.

Marks, M.J., P.P. Rowell, J.Z. Cao, S.R. Grady, S.E. McCallum, and A.C. Collins. 2004. Subsets of acetylcholine-stimulated $^{86}Rb^+$ efflux and [^{125}I]-epibatidine binding sites in C57BL/6 mouse brain are differentially affected by chronic nicotine treatment. *Neuropharmacology.* 46:1141–1157. http://dx.doi.org/10.1016/j.neuropharm.2004.02.009

Miesenböck, G., D.A. De Angelis, and J.E. Rothman. 1998. Visualizing secretion and synaptic transmission with pH-sensitive green fluorescent proteins. *Nature.* 394:192–195. http://dx.doi.org/10.1038/28190

Miwa, J.M., R. Freedman, and H.A. Lester. 2011. Neural systems governed by nicotinic acetylcholine receptors: emerging hypotheses. *Neuron.* 70:20–33. http://dx.doi.org/10.1016/j.neuron.2011.03.014

Miwa, J.M., H.A. Lester, and A. Walz. 2012. Optimizing cholinergic tone through lynx modulators of nicotinic receptors: implications for plasticity and nicotine addiction. *Physiology (Bethesda).* 27:187–199. http://dx.doi.org/10.1152/physiol.00002.2012

Moss, F.J., P.I. Imoukhuede, K. Scott, J. Hu, J.L. Jankowsky, M.W. Quick, and H.A. Lester. 2009. GABA transporter function, oligomerization state, and anchoring: Correlates with subcellularly resolved FRET. *J. Gen. Physiol.* 134:489–521. http://dx.doi.org/10.1085/jgp.200910314

Mukhin, A.G., A.S. Kimes, S.I. Chefer, J.A. Matochik, C.S. Contoreggi, A.G. Horti, D.B. Vaupel, O. Pavlova, and E.A. Stein. 2008. Greater nicotinic acetylcholine receptor density in smokers than in nonsmokers: a PET study with 2-18F-FA-85380. *J. Nucl. Med.* 49:1628–1635. http://dx.doi.org/10.2967/jnumed.108.050716

Nashmi, R., C. Xiao, P. Deshpande, S. McKinney, S.R. Grady, P. Whiteaker, Q. Huang, T. McClure-Begley, J.M. Lindstrom, C. Labarca, et al. 2007. Chronic nicotine cell specifically upregulates functional α4* nicotinic receptors: basis for both tolerance in midbrain and enhanced long-term potentiation in perforant path. *J. Neurosci.* 27:8202–8218. http://dx.doi.org/10.1523/JNEUROSCI.2199-07.2007

Nguyen, H.N., B.A. Rasmussen, and D.C. Perry. 2004. Binding and functional activity of nicotinic cholinergic receptors in selected rat brain regions are increased following long-term but not short-term nicotine treatment. *J. Neurochem.* 90:40–49. http://dx.doi.org/10.1111/j.1471-4159.2004.02482.x

Orci, L., M. Stamnes, M. Ravazzola, M. Amherdt, A. Perrelet, T.H. Söllner, and J.E. Rothman. 1997. Bidirectional transport by distinct populations of COPI-coated vesicles. *Cell.* 90:335–349. http://dx.doi.org/10.1016/S0092-8674(00)80341-4

Parker, S.L., Y. Fu, K. McAllen, J. Luo, J.M. McIntosh, J.M. Lindstrom, and B.M. Sharp. 2004. Up-regulation of brain nicotinic acetylcholine receptors in the rat during long-term self-administration of nicotine: disproportionate increase of the α6 subunit. *Mol. Pharmacol.* 65:611–622. http://dx.doi.org/10.1124/mol.65.3.611

Peng, X., V. Gerzanich, R. Anand, P.J. Whiting, and J. Lindstrom. 1994. Nicotine-induced increase in neuronal nicotinic receptors results from a decrease in the rate of receptor turnover. *Mol. Pharmacol.* 46:523–530.

Perez, X.A., T. Bordia, J.M. McIntosh, S.R. Grady, and M. Quik. 2008. Long-term nicotine treatment differentially regulates striatal α6α4β2* and α6(nonα4)β2* nAChR expression and function. *Mol. Pharmacol.* 74:844–853. http://dx.doi.org/10.1124/mol.108.048843

Perry, D.C., D. Mao, A.B. Gold, J.M. McIntosh, J.C. Pezzullo, and K.J. Kellar. 2007. Chronic nicotine differentially regulates α6- and β3-containing nicotinic cholinergic receptors in rat brain. *J. Pharmacol. Exp. Ther.* 322:306–315. http://dx.doi.org/10.1124/jpet.107.121228

Picciotto, M.R., M. Zoli, R. Rimondini, C. Léna, L.M. Marubio, E.M. Pich, K. Fuxe, and J.P. Changeux. 1998. Acetylcholine receptors containing the β2 subunit are involved in the reinforcing properties of nicotine. *Nature.* 391:173–177. http://dx.doi.org/10.1038/34413

Pons, S., L. Fattore, G. Cossu, S. Tolu, E. Porcu, J.M. McIntosh, J.P. Changeux, U. Maskos, and W. Fratta. 2008. Crucial role of α4 and α6 nicotinic acetylcholine receptor subunits from ventral tegmental area in systemic nicotine self-administration. *J. Neurosci.* 28:12318–12327. http://dx.doi.org/10.1523/JNEUROSCI.3918-08.2008

Rauhut, A.S., N. Neugebauer, L.P. Dwoskin, and M.T. Bardo. 2003. Effect of bupropion on nicotine self-administration in rats. *Psychopharmacology (Berl.).* 169:1–9. http://dx.doi.org/10.1007/s00213-003-1450-x

Richards, C.I., R. Srinivasan, C. Xiao, E.D. Mackey, J.M. Miwa, and H.A. Lester. 2011. Trafficking of α4* nicotinic receptors revealed by superecliptic phluorin: effects of a β4 amyotrophic lateral sclerosis-associated mutation and chronic exposure to nicotine. *J. Biol. Chem.* 286:31241–31249. http://dx.doi.org/10.1074/jbc.M111.256024

Ritz, B., A. Ascherio, H. Checkoway, K.S. Marder, L.M. Nelson, W.A. Rocca, G.W. Ross, D. Strickland, S.K. Van Den Eeden, and J. Gorell. 2007. Pooled analysis of tobacco use and risk of Parkinson disease. *Arch. Neurol.* 64:990–997. http://dx.doi.org/10.1001/archneur.64.7.990

Sallette, J., S. Pons, A. Devillers-Thiery, M. Soudant, L. Prado de Carvalho, J.P. Changeux, and P.J. Corringer. 2005. Nicotine upregulates its own receptors through enhanced intracellular maturation. *Neuron.* 46:595–607. http://dx.doi.org/10.1016/j.neuron.2005.03.029

Schnoll, R.A., E.P. Wileyto, F.T. Leone, R.F. Tyndale, and N.L. Benowitz. 2013. High dose transdermal nicotine for fast metabolizers of nicotine: a proof of concept placebo-controlled trial. *Nicotine Tob. Res.* 15:348–354. http://dx.doi.org/10.1093/ntr/nts129

Schwartz, R.D., and K.J. Kellar. 1983. Nicotinic cholinergic receptor binding sites in the brain: regulation in vivo. *Science.* 220:214–216. http://dx.doi.org/10.1126/science.6828889

Spang, A. 2013. Traffic COPs: rules of detection. *EMBO J.* 32:915–916. http://dx.doi.org/10.1038/emboj.2013.57

Srinivasan, R., R. Pantoja, F.J. Moss, E.D.W. Mackey, C.D. Son, J. Miwa, and H.A. Lester. 2011. Nicotine up-regulates α4β2 nicotinic receptors and ER exit sites via stoichiometry-dependent chaperoning. *J. Gen. Physiol.* 137:59–79. http://dx.doi.org/10.1085/jgp.201010532

Srinivasan, R., C.I. Richards, C. Dilworth, F.J. Moss, D.A. Dougherty, and H.A. Lester. 2012a. Förster resonance energy transfer (FRET) correlates of altered subunit stoichiometry in Cys-loop receptors, exemplified by nicotinic α4β2. *Int. J. Mol. Sci.* 13:10022–10040. http://dx.doi.org/10.3390/ijms130810022

Srinivasan, R., C.I. Richards, C. Xiao, D. Rhee, R. Pantoja, D.A. Dougherty, J.M. Miwa, and H.A. Lester. 2012b. Pharmacological chaperoning of nicotinic acetylcholine receptors reduces the endoplasmic reticulum stress response. *Mol. Pharmacol.* 81:759–769. http://dx.doi.org/10.1124/mol.112.077792

Tapper, A.R., S.L. McKinney, R. Nashmi, J. Schwarz, P. Deshpande, C. Labarca, P. Whiteaker, M.J. Marks, A.C. Collins, and H.A. Lester. 2004. Nicotine activation of α4* receptors: sufficient for reward, tolerance, and sensitization. *Science.* 306:1029–1032. http://dx.doi.org/10.1126/science.1099420

Tumkosit, P., A. Kuryatov, J. Luo, and J. Lindstrom. 2006. β3 subunits promote expression and nicotine-induced up-regulation of human nicotinic α6* nicotinic acetylcholine receptors expressed in transfected cell lines. *Mol. Pharmacol.* 70:1358–1368. http://dx.doi.org/10.1124/mol.106.027326

Walsh, H., A.P. Govind, R. Mastro, J.C. Hoda, D. Bertrand, Y. Vallejo, and W.N. Green. 2008. Up-regulation of nicotinic receptors by nicotine varies with receptor subtype. *J. Biol. Chem.* 283:6022–6032. http://dx.doi.org/10.1074/jbc.M703432200

Watkins, S.S., M.P. Epping-Jordan, G.F. Koob, and A. Markou. 1999. Blockade of nicotine self-administration with nicotinic antagonists in rats. *Pharmacol. Biochem. Behav.* 62:743–751. http://dx.doi.org/10.1016/S0091-3057(98)00226-3

Whiteaker, P., C.G. Sharples, and S. Wonnacott. 1998. Agonist-induced up-regulation of α4β2 nicotinic acetylcholine receptors in M10 cells: pharmacological and spatial definition. *Mol. Pharmacol.* 53:950–962.

Xiao, C., R. Srinivasan, R.M. Drenan, E.D. Mackey, J.M. McIntosh, and H.A. Lester. 2011. Characterizing functional α6β2 nicotinic acetylcholine receptors in vitro: mutant β2 subunits improve membrane expression, and fluorescent proteins reveal responsive cells. *Biochem. Pharmacol.* 82:852–861. http://dx.doi.org/10.1016/j.bcp.2011.05.005

Yang, J.S., S.Y. Lee, S. Spanò, H. Gad, L. Zhang, Z. Nie, M. Bonazzi, D. Corda, A. Luini, and V.W. Hsu. 2005. A role for BARS at the fission step of COPI vesicle formation from Golgi membrane. *EMBO J.* 24:4133–4143. http://dx.doi.org/10.1038/sj.emboj.7600873

Yang, J.S., C. Valente, R.S. Polishchuk, G. Turacchio, E. Layre, D.B. Moody, C.C. Leslie, M.H. Gelb, W.J. Brown, D. Corda, et al. 2011. COPI acts in both vesicular and tubular transport. *Nat. Cell Biol.* 13:996–1003. http://dx.doi.org/10.1038/ncb2273

Yoshimura, R.F., D.J. Hogenkamp, W.Y. Li, M.B. Tran, J.D. Belluzzi, E.R. Whittemore, F.M. Leslie, and K.W. Gee. 2007. Negative allosteric modulation of nicotinic acetylcholine receptors blocks nicotine self-administration in rats. *J. Pharmacol. Exp. Ther.* 323:907–915. http://dx.doi.org/10.1124/jpet.107.128751